NASA Contractor Report 166055

(NASA-CR-166055) ATOPS B-737 INNER-LOOP CONTROL SYSTEM LINEAR MODEL CONSTRUCTION AND VERIFICATION Interim Report (Information and Control Systems, Inc.) 65 p HC A04/MF A01 CSCL 01C G3/08

N84-10078

Unclas 30031

ATOPS B-737 INNER-LOOP CONTROL SYSTEM

LINEAR MODEL CONSTRUCTION AND VERIFICATION

John R. Broussard

INFORMATION & CONTROL SYSTEMS, INCORPORATED
Hampton, Virginia 23666

Contract NAS1-15759
February 1983

National Aeronautics and
Space Administration

Langley Research Center
Hampton, Virginia 23665

TABLE OF CONTENTS

LIST OF TABLES

LIST OF FIGURES

LIST OF FIGURES (CONTINUED)

I. INTRODUCTION

An outer-loop control system synthesis procedure is currently undergoing development. A description of the approach is given in Ref. 1. The outer-loop synthesis procedure is being applied to a 3-D R/NAV control design problem for the NASA ATOPS B-737 research aircraft.

The outer-loop design approach requires an operational inner-loop control system before the outer-loop feedback gains can be determined. The inner-loop control system employed is a derivative the Boeing control system documented in Refs. 2 - 7. The advantage of using the Boeing design is that is has been extensively analyzed and flight tested.

To facilitate the design process, a linear model of the inner-loop control system is required. This technical note presents the linear and nonlinear models of the Boeing inner-loop control system. Validation of the linear model is determined by comparing linear and nonlinear simulations.

There are two approaches which can be used in representing the inner-loop control system. The easiest approach, and the method used in this report, is to model the inner-loop control system in continuous time and combine the resulting equations with the linear models of the aircraft and actuators, to obtain

$$\Delta\dot{\underline{x}}_{CL} = A_{CL}\Delta\underline{x}_{CL} + B_{CL}\Delta\underline{u}_{CL} + E_{CL}\Delta\underline{w}_{CL} \qquad (1)$$

The states are the n-vector, $\underline{x}_{CL}$, the outer-loop controls are the m-vector, $\underline{u}_{CL}$, and the disturbances are the d-vector, $\Delta\underline{w}_{CL}$. A_{CL}, B_{CL}, and E_{CL} are constant matrices of appropriate dimension. The discrete model for the outer-loop design becomes

$$\Delta\underline{x}_{CK,k+1} = \Phi_{CL}\Delta\underline{x}_{CL,k} + \Gamma_{CL}\Delta\underline{u}_{CL,k} + \Upsilon_{CL}\Delta\underline{w}_{CL,k} \tag{2}$$

where

$$\Phi_{CL} = e^{A_{CL}\Delta t} \tag{3}$$

$$\Gamma_{CL} = \int_0^{\Delta t} e^{A_{CL}s}\, ds\, G_{CL}, \quad \Upsilon_{CL}\Delta\underline{w}_{CL,k} = \int_0^{\Delta t} e^{A_{CL}s}\, E_{CL}\Delta\underline{w}_{CL}(s)\, ds \tag{4}$$

The sampling time, Δt, can be chosen as desired.

The second and more accurate approach is to model the plant and actuator dynamics in continuous-time as before but model the inner control system in discrete time. The assumptions used in digitally implementing the inner-loop control system (trapezoidal integration, measurement and computation delays, Tustin's transformation, sampling time $\simeq$ 0.05 sec) are accounted for in the discrete model. A discrete representation of the plant is combined with the discrete inner-loop control law system to produce Eq. 2. If the outer-loop control system is to operate at a slower rate (Δt = 0.1 sec), the control design becomes multirate. Techniques for handling multirate multivariable control designs have recently been determined in Ref. 8 but are outside the scope of this work. The second approach represents future schemes which may be useful if more accurate evaluation techniques become necessary.

The report is organized into six chapters. Chapter two presents nonlinear block diagrams of the inner-loop control laws and the corresponding linear time-invariant equations of the inner-loop models. Chapter three details the steps used in linearizing the inner-loop control laws. Chapter four combines the linear inner-loop models into the continuous-time plant representation shown in Eq. 1. The properties of proportional plus integral feedback of acceleration error in the inner-loop control laws are also discussed in Chapter four. Chapter five presents simulations comparing linear model time histories with nonlinear model time histories. The report is summarized in Chapter six. Appendix A compares nonlinear ACSL simulations with a recently developed ATOPS B-737 FORTRAN simulation.

II. INNER-LOOP MODELS

A. AUTOTHROTTLE

The autothrottle inner-loop is the most complicated of the control designs. Two error signals are computed and compared to threshold values. Control feedback paths are switched on and off as the error signals cross the threshold values. A windshear estimator is used to produce feedback for windshear compensation. The versine of the roll angle is fed back to advance the throttle just as the airplane rolls into a turn. The roll angle signal is washed out to prevent throttle advance in a steady turn. A block diagram of the autothrottle inner-loop control system is shown in Fig. 1. The gains in the block diagram are defined in Table 1.

A detailed explanation of the windshear estimator is given in Ref. 3. Basically, true airspeed, TAS and longitudinal acceleration, $\dot{V}_{GS}$, are employed in a complementary filter to produce $\dot{V}_{CF}$ where

$$\dot{V}_{CF} = -V_W \frac{s}{\frac{1.0}{k_{10}} s + 1} \tag{5}$$

V_W is the wind velocity making $\dot{V}_{CF}$ a washed-out estimate of wind. $\dot{V}_{CF}$ is next passed through a wind turbulence filter to filter out high frequency components in $\dot{V}_{CF}$,

$$\hat{\dot{V}}_{CF} = \frac{k_{12}}{s} \text{ Bound } \frac{+k_{11}}{-k_{11}} (\hat{\dot{V}}_{CF} - \hat{\dot{V}}_{CF}) \tag{6}$$

The negative wind shear estimate, $\dot{V}_{CF}$, is subtracted from $\dot{V}_{GS}$ to form the acceleration feedback signal. The acceleration feedback signal is

subtracted from the acceleration command, $\ddot{x}_c$, to form the command error. The integral of the command error becomes one of the feedback paths to the incremental throttle command δ_{TC}.

If the engine pressure ratio (EPR) approaches the maximum safe value for EPR (MXEPR), special logic, (switch B as shown in Fig. 1) switches the EPR error signal to input the throttle integrator. The effect is to cause a decrease in the incremental throttle command. Switch A causes a throttle down error command to immediately decrease the rate of change of the throttle integrator.

A linear model for autothrottle is as follows

$$\begin{bmatrix} \Delta\dot{\hat{V}}_{CF} \\ \Delta\dot{\hat{V}}_{I} \\ \Delta\dot{\xi}_{x} \\ \Delta\dot{\phi}_{WO} \end{bmatrix} = \begin{bmatrix} -k_{12} & k_{10}*k_{12} & 0.0 & 0.0 \\ 0.0 & -k_{10} & 0.0 & 0.0 \\ k_7 Y & 0.0 & 0.0 & k_7 Y \\ 0.0 & 0.0 & 0.0 & -1.0/k_2 \end{bmatrix} \begin{bmatrix} \Delta\dot{\hat{V}}_{CF} \\ \Delta\hat{V}_{I} \\ \Delta\xi_{x} \\ \Delta\phi_{WO} \end{bmatrix}$$

$$+ \begin{bmatrix} 0.0 & -k_{10}*k_{12} & 0.0 \\ 1.0 & k_{10} & 0.0 \\ -k_7 Y & 0.0 & k_1*k_7 \sin\phi_o \\ 0.0 & 0.0 & -k_1/k_2 \sin\phi_o \end{bmatrix} \begin{bmatrix} \Delta\dot{V}_{GS}+\Delta\nu_{GS} \\ \Delta V_{TAS}+\Delta\nu_{TAS} \\ \Delta\phi+\Delta\nu_{\phi} \end{bmatrix}$$

$$+ \begin{bmatrix} 0.0 \\ 0.0 \\ k_7 Y \\ 0.0 \end{bmatrix} \begin{bmatrix} \Delta\ddot{x}_c \end{bmatrix} \qquad (7)$$

$$\Delta\delta_{TC} = \begin{bmatrix} k_9 & 0.0 & 1.0 & 0.0 \end{bmatrix} \begin{bmatrix} \Delta\hat{\dot{V}}_{CF} \\ \Delta\hat{V}_I \\ \Delta\xi_x \\ \Delta\phi_{WO} \end{bmatrix} + \begin{bmatrix} -k_9 & 0.0 & 0.0 \end{bmatrix} \begin{bmatrix} \Delta\dot{V}_{GS}+\Delta\nu_{GS} \\ \Delta V_{TAS}+\Delta\nu_{TAS} \\ \Delta\phi+\Delta\nu_{\phi} \end{bmatrix}$$

$$+ [0.0][\Delta\ddot{x}_c] \tag{7}$$

The state $\Delta\xi_x$ is the integral of perturbation command error. The state $\Delta\phi_{WO}$ is the perturbation washed out versine roll correction factor. The acceleration measurement, $\Delta\dot{V}_{GS}$, is the perturbation rate of change of ground speed. ΔV_{TAS} is the measured perturbation true airspeed. $\Delta\phi$ is the measured perturbation roll angle and $\Delta\ddot{x}_c$ is the perturbation outer-loop command. In straight and level flight, the versine roll correction state can be eliminated. The variable, Y, in Eq. 7 is an option to account for switch A as follows

$$e_{EPR} = MXEPR - 0.1 - EPR_o \tag{9}$$

$$Z = \begin{cases} k_4 & e_{EPR} > k_3 \\ (k_4/k_3)*e_{EPR} & 0.0 < e_{EPR} < k_3 \\ 0.0 & e_{EPR} < 0.0 \end{cases} \tag{10}$$

$$\text{OPTION 1, } A > 0, \quad Y = Z \tag{11}$$

$$\text{OPTION 2, } A < 0, \quad Y = 1.0 \tag{12}$$

For a given trim flight conditions, outer-loop gains could be determined first for OPTION 1 then for OPTION 2. If noticable changes are apparant, the effect of A may have to be accommodated in the outer-loop control law. The nonlinear bounds caused by the gains k_6, k_{11}, k_{13} and k_8 are

neglected when the linear model is constructed in Eq. 7. An approach using describing functions shown later in Eq. 18 could be used to model nonlinear bounds in the linear plant representation. The variables Δv_{GS}, Δv_{TAS} and Δv_{ϕ} are measurement noise.

B. VERTICAL PATH

A block diagram of the vertical path inner-loop for the elevator is shown in Fig. 2. The gains are given in Table 2. Neither the elevator inner-loop, nor the autothrottle inner-loop employ pitch attitude feedback for stability during path tracking. Reference 3 explains that replacing a pitch attitude command system with a vertical acceleration command system allows the aircraft to weather cock vertically upon encountering vertical gusts and shears so that glideslope beam tracking performance can be enhanced. Other types of control design procedures can produce an elevator control system that weather cocks, employs pitch attitude feedback, and has good glideslope tracking performance as discussed in Ref. 9.

The elevator inner-loop filters the vertical acceleration measurement, forms the acceleration command error, then feeds the error signal in proportional-integral form to the elevator. The integrator output is position limited. Washed-out pitch rate is fed back for improved stability. The vertical acceleration command is position limited to insure passenger comfort. The feedback signal to elevator is multiplied by a gain that decreases with increasing calibrated airspeed. The linear model for elevator is

$$\begin{bmatrix} \Delta\dot{\underline{q}}_{WO} \\ \Delta\dot{\hat{\ddot{h}}} \\ \Delta\dot{\xi}_h \end{bmatrix} = \begin{bmatrix} -1.0/k_{28} & 0.0 & 0.0 \\ 0.0 & -1.0/k_{20} & 0.0 \\ 0.0 & k_{24}*k_{22} & 0.0 \end{bmatrix} \begin{bmatrix} \Delta\underline{q}_{WO} \\ \Delta\hat{\ddot{h}} \\ \Delta\xi_h \end{bmatrix}$$

$$+ \begin{bmatrix} -1.0/k_{28} & 0.0 \\ 0.0 & 1.0/k_{20} \\ 0.0 & 0.0 \end{bmatrix} \begin{bmatrix} \Delta\underline{q} + \Delta\nu_{\underline{q}} \\ \Delta\ddot{h} + \Delta\nu_{\ddot{h}} \end{bmatrix} + \begin{bmatrix} 0.0 \\ 0.0 \\ -k_{24}*k_{22} \end{bmatrix} [\Delta\ddot{h}_C] \qquad (13)$$

$$\Delta\delta_{EC} = K_{CAS}[k_{27} \quad k_{25}*k_{22} \quad k_{25}] \begin{bmatrix} \Delta\underline{q}_{WO} \\ \Delta\hat{\ddot{h}} \\ \Delta\xi_h \end{bmatrix} + K_{CAS}[k_{27} \quad 0.0 \begin{bmatrix} \Delta\underline{q} + \Delta\nu_{\underline{q}} \\ \Delta\ddot{h} + \Delta\nu_{\ddot{h}} \end{bmatrix}$$

$$+ K_{CAS}[-k_{25}*k_{22}] [\Delta\ddot{h}_c] \qquad (14)$$

The perturbation states are the integral of command error, $\Delta\xi_h$, filtered vertical acceleration, $\Delta\hat{\ddot{h}}$, and washed out pitch rate, $\Delta\underline{q}_{WO}$. The measurements are pitch rate, $\Delta\underline{q}$, and INS (Invertial Naviation System) vertical acceleration, $\Delta\ddot{h}$. The outer-loop control input is the vertical acceleration command, $\Delta\ddot{h}_C$. The limit on $\Delta\ddot{h}_C$ could be handled similiar to Eq. 18.

C. HORIZONTAL PATH

The horizontal path inner-loop feeds back roll rate for stability augmentation and the error between the outer-loop roll angle command and roll angle. A block diagram of the control law is shown in Fig. 3. The gain values are defined in Table 3. The feedback signal which forms the aileron actuator command is multiplied by the gain k_v which is a function of calibrated airspeed, CAS, as shown in Fig. 3. The roll command signal is limited.

A linear model of the horizontal path inner-loop which accounts for the roll command rate limit is

$$\begin{bmatrix} \Delta\hat{p} \\ \Delta\hat{\phi}_C \end{bmatrix} = \begin{bmatrix} -1.0/k_{32} & 0.0 & \Delta\hat{p} \\ 0.0 & -k_{36}J & \Delta\hat{\phi}_C \end{bmatrix} + \begin{bmatrix} 1.0/k_{32} & 0.0 \\ 0.0 & 0.0 \end{bmatrix} \begin{bmatrix} \Delta p + \Delta\nu_p \\ \ddot{\Delta\phi} + \Delta\nu_\phi \end{bmatrix}$$

$$+ \begin{bmatrix} 0.0 \\ k_{36}J \end{bmatrix} \begin{bmatrix} \Delta\phi_C \end{bmatrix} \tag{15}$$

$$\Delta\delta_{AC} = [-k_v*k_{33} \quad k_v*k_{38}] \begin{bmatrix} \Delta\hat{p} \\ \Delta\hat{\phi}_C \end{bmatrix} + [0.0 \quad k_v*k_{33}] \begin{bmatrix} \Delta\hat{p} + \Delta\nu_p \\ \Delta\phi + \Delta\nu_\phi \end{bmatrix}$$

$$+ [0.0][\Delta\phi_C] \tag{16}$$

The perturbation states are filtered roll rate, $\Delta\hat{p}$, and filtered roll command, $\Delta\hat{\phi}_C$. The measurementas are roll rate, Δp, and roll angle $\Delta\phi$. The outer-loop control input is the roll command, $\Delta\phi_C$.

Using describing functions, if $\Delta\phi_C$ changes abruptly then

$$A = \Delta\phi_C - \Delta\hat{\phi}_C = \phi_C - \hat{\phi}_C \tag{17}$$

$$J = \begin{cases} 1.0 & |A| \le k_{37} \\ \dfrac{1.0}{\pi}\left(\left|\dfrac{4}{A}\right|\sqrt{1-\left|\dfrac{4}{A}\right|^2} + 2\sin^{-1}\left|\dfrac{4}{A}\right|\right) & |A| > k_{37} \end{cases} \tag{18}$$

The advantage of allowing J to be variable is that outer-loop guidance gains can be designed for different values of A.

D. RUDDER

The Boeing inner-loop control system for rudder is the yaw damper shown in Fig. 4. The gains are shown in Table 4. Body axis yaw rate

is filtered to suppress measurement noise. The filtered yaw rate is multiplied by a gain which is a function of CAS as shown in Table 5. to decrease the gain as airspeed increases. The filtered yaw rate signal is washed out for turn coordination then position limited to reduce control authority. Outer-loop commands directly actuate the rudder surface. The Boeing outer-loop control design commands rudder for decrab during landings.

The linear model of the inner-loop is

$$\begin{bmatrix} \Delta\dot{r}_{WO} \\ \Delta\dot{\hat{r}} \end{bmatrix} = \begin{bmatrix} -1.0/k_{42} & -1.0/k_{42} \\ 0.0 & -1.0/k_{41} \end{bmatrix} \begin{bmatrix} \Delta r_{WO} \\ \Delta\hat{r} \end{bmatrix} + \begin{bmatrix} 0 \\ KYD*k_{40}/k_{41} \end{bmatrix} (\Delta r + \Delta v_r) \quad (19)$$

$$\Delta\delta_{RC} = [1.0 \quad 1.0] \begin{bmatrix} \Delta r_{WO} \\ \Delta\hat{r} \end{bmatrix} + [0.0][\Delta r + \Delta v_r] + [1.0][\Delta u_C] \quad (20)$$

The position limits in Fig. 4 could similarily be incorporated in the linear model using Eq. 18 if this is deemed desirable. The perturbation states in the linear model are filtered yaw rate, $\Delta\hat{r}$, and washed out yaw rate, Δr_{WO}. The measurement is yaw rate, Δr. The outer-loop control is Δu_{RC}.

III. LINEAR MODEL ANALYSIS

A. LINEARIZATION OF FEEDBACK ELEMENTS

The Boeing inner-loop system uses the derivative of ground speed, $\dot{V}_{GS}$, true airspeed, V_{TAS}, and vertical acceleration, $\ddot{h}$ as feedback elements. Linear analyisis requires that these elements be linearized and expressed in terms of the perturbed states and controls of the aircraft. This section derives the perturbation relationships.

Figure 5 shows the relationships between the accelerations of the vehicle in a local-level north pointing frame and the along track and cross track accelerations. The north pointing frame is denoted as the geographic coordinate system. In the figure, V_G is the ground speed, a is the vehicle acceleration in the horizontal plane, and ξ is the ground track angle.

From the figure it follows that

$$\tan = \frac{\dot{y}}{\dot{x}} \quad , \qquad V_G = (\dot{x}^2 + \dot{y}^2)^{\frac{1}{2}} \tag{21a, b}$$

The along track, a_{ATK}, and cross track, a_{CTK}, accelerations are related to $\ddot{x}$ and $\ddot{y}$ through the transformation,

$$\begin{bmatrix} a_{ATK} \\ a_{CTK} \end{bmatrix} = \begin{bmatrix} \cos\xi & \sin\xi \\ -\sin\xi & \cos\xi \end{bmatrix} \begin{bmatrix} \ddot{x} \\ \ddot{y} \end{bmatrix} \tag{22}$$

Expressing $\cos\xi$ and $\sin\xi$ in terms of $\dot{x}$ and $\dot{y}$ the following occurs

$$a_{ATK} = \frac{\dot{x}\ddot{x} + \dot{y}\ddot{y}}{V_G} \tag{23}$$

$$a_{CTK} = \frac{\dot{x}\ddot{y} - \dot{y}\ddot{x}}{V_G} \tag{24}$$

Note that taking the derivative of V_G in Eq. 21b, shows that $\dot{V}_G$ and a_{ATK} in Eq. 23 are equal as required. Perturbing Eq. 24 produces

$$\Delta\dot{V}_G = \begin{bmatrix} \frac{V_{Go}\,\ddot{x}_o - \dot{V}_{Go}\,\dot{x}_o}{V_{Go}^2} & \frac{V_{Go}\,\ddot{y} - \dot{V}_{Go}\,\dot{y}}{V_{Go}^2} & 0 \end{bmatrix} \begin{bmatrix} \Delta\dot{x} \\ \Delta\dot{y} \\ \Delta\dot{z} \end{bmatrix}$$

$$+ \begin{bmatrix} \frac{\dot{x}_o}{V_{Go}} & \frac{\dot{y}_o}{V_{Go}} & 0 \end{bmatrix} \begin{bmatrix} \Delta\ddot{x} \\ \Delta\ddot{y} \\ \Delta\ddot{z} \end{bmatrix} \tag{25}$$

which is rewritten in matrix form as

$$\dot{V}_G = H_{\dot{x}} \,\underline{\Delta\dot{x}} + H_{\ddot{x}} \,\underline{\Delta\ddot{x}} \tag{26}$$

Let $H_G^B(\phi,\theta,\psi)$ be the transformation from body axes to geographic axes where ϕ, θ, and ψ are the Euler angles (platform axes and geographic axes are assumed to coincide). It follows that

$$H_B^G = H_G^{B\,T} \tag{27}$$

$$\underline{\dot{x}} = H_B^G \,\underline{v}_B \tag{28}$$

where

$$\underline{v}_B^T = [u \quad v \quad w] \tag{29}$$

and

$$\underline{\ddot{x}} = H_B^G \,\underline{\dot{v}}_B + H_B^G \,\tilde{\omega}_B^G \,\underline{v}_B \tag{30}$$

The vector ω_B^G represents the body axis angular rates in radians, (a flat nonrotating earth is assumed)

$$\omega_B^{G\,T} = [p \quad q \quad r] \tag{31}$$

$\tilde{\omega}_B^G$ is the matrix representation of the vector cross product and is given by

$$\tilde{\omega}_B^G = \begin{bmatrix} 0 & -r & q \\ r & 0 & -p \\ -q & p & 0 \end{bmatrix} \tag{32}$$

Perturbing Eq. 28 produces

$$\Delta\underline{\dot{x}} = H_{B_o}^G \, \Delta\underline{v}_B - \widetilde{(\dot{x}_o)} \, H_{B_o}^G \, L_{B_o} \, \Delta\underline{\nu}_B \tag{33}$$

where

$$L_{B_o} = \begin{bmatrix} 1.0 & 0.0 & -\sin\theta_o \\ 0.0 & \cos\phi_o & \sin\phi_o\cos\theta_o \\ 0.0 & -\sin\phi_o & \cos\phi_o\cos\theta_o \end{bmatrix} \tag{34}$$

and

$$\Delta\underline{\nu}_B^T = [\Delta\phi \quad \Delta\theta \quad \Delta\psi] \tag{35}$$

Perturbing Eq. 30 produces

$$\begin{aligned} \Delta\underline{\ddot{x}} = {} & H_{B_o}^G \, \Delta\underline{\dot{v}}_B - \tilde{\dot{x}}_o H_{B_o}^G \, K_{B_o} \, \Delta\underline{\nu}_B + H_{B_o}^G \, \tilde{\omega}_B^G \, \Delta\underline{v}_B \\ & + \widetilde{(\dot{x}_o - \ddot{x}_o)} \, H_{B_o}^G \, L_{B_o} \, \Delta\underline{\nu}_B - H_{B_o}^G \, \tilde{v}_B \Delta\underline{\omega}_B^E \end{aligned} \tag{36}$$

A expression for $\Delta\underline{\dot{v}}_B$ can be determined from the linear aerodynamic model

of the aircraft,

$$\Delta\dot{\underline{x}} = A\,\Delta\underline{x} + B\,\Delta\underline{u} + E\,\Delta\underline{w}_g \tag{37}$$

Extracting the equation for $\Delta\dot{\underline{v}}_B$ from Eq. 37 produces

$$\Delta\dot{\underline{v}}_B = [A_{vv} \quad A_{v\omega} \quad A_{v\nu}]\begin{bmatrix}\Delta\underline{v}_B \\ \Delta\underline{\omega}_B^G \\ \Delta\underline{\nu}_B\end{bmatrix} + B_{vu}\,\Delta\underline{u} + E_{vw}\,\Delta\underline{w}_g \tag{38}$$

The states, $\Delta\underline{w}$ are gust disturbances. Substituting Eq. 37 into Eq. 36 results in

$$\begin{aligned}\Delta\ddot{\underline{x}} = {} & (H_{B_o}^G A_{vv} + H_{B_o}^G \tilde{\omega}_B^G)\,\Delta\underline{v}_B + (H_{B_o}^E A_{v\omega} - H_{B_o}^E \tilde{\underline{v}}_{B_o})\,\Delta\underline{\omega}_B^G \\ & + (\widetilde{(\dot{\underline{x}}_o - \ddot{\underline{x}}_o)}\, H_{B_o}^G L_{B_o} - \tilde{\dot{\underline{x}}}_o H_{B_o}^G L_{B_o} + H_{B_o}^G F_{v\nu})\,\Delta\underline{\nu}_B \\ & + H_{B_o}^G B_{vu}\,\Delta\underline{u} + H_{B_o} E_{vw}\,\Delta\underline{w}_g\end{aligned} \tag{39}$$

Substituting Eq. 33 and Eq. 39 into Eq. 36 determines the desired equation for $\dot{V}_G$ in terms of the aircraft perturbation states and controls,

$$\Delta\dot{V}_G = H_{vv}\Delta\underline{v}_B + H_{v\omega}\Delta\underline{\omega}_B^G + H_{v\nu}\Delta\underline{\nu}_B + D_{vu}\Delta\underline{u} + D_{vw}\Delta\underline{w} \tag{40}$$

where

$$H_{vv} = H_{\underline{x}}H_{B_o}^G + H_{\underline{\dot{x}}}H_1 \tag{41}$$

$$H_1 = H_{B_o}^G A_{vv} + H_{B_o}^G \tilde{\omega}_B^E \tag{42}$$

$$H_{vw} = H_{\underline{\dot{x}}}H_2 \tag{43}$$

$$H_2 = H^G_{B_o} (A_{v\omega} - \tilde{v}_{B_o}) \tag{44}$$

$$H_{v\nu} = H_{\dot{x}} (-\widetilde{(\dot{x}_o)} H^G_{B_o} L_{B_o}) + H_{\ddot{x}} H_3 \tag{45}$$

$$H_3 = [\widetilde{(\dot{x}_o - \ddot{x}_o)} - \tilde{\dot{x}}_o] H^G_{B_o} L_B + H^G_{B_o} F_{v\nu} \tag{46}$$

$$D_{vu} = H_{\ddot{x}} H_4 \tag{47}$$

$$H_4 = H^G_{B_o} B_{vu} \tag{48}$$

$$D_{vw} = H_{\ddot{x}} H_5 \tag{49}$$

$$H_5 = H^G_{B_o} E_{vw} \tag{50}$$

A similiar expression for $\Delta\ddot{h}$ is obtained by noting that

$$\Delta\ddot{h} = H_h^{\cdot\cdot} \Delta\ddot{x} \tag{51}$$

where

$$H_h^{\cdot\cdot} = [0 \; 0 \; -1] \tag{52}$$

Substituting Eq. 39 into Eq. 51 determines the desired perturbation expression for $\Delta\ddot{h}$ in terms of the perturbation aircraft states and controls.

$$\Delta\ddot{h} = H_h H_1 \Delta\underline{v}_B + H_h H_2 \Delta\underline{\omega}^G_B + H_h H_3 \Delta\underline{\nu}_B + H_h H_4 \Delta\underline{u} + H_h H_5 \Delta\underline{w} \tag{53}$$

True airspeed is the velocity of the vehicle relative to the atmosphere,

$$V_{TAS} = (u_A^2 + v_A^2 + w_A^2)^{\frac{1}{2}} \tag{54}$$

$$\underline{v}_A = \begin{bmatrix} u_A \\ v_A \\ w_A \end{bmatrix} \tag{55}$$

$$\underline{v}_A = \underline{v}_B - H_G^B \underline{w}_E - \underline{w} \tag{56}$$

The vector $\underline{w}_E$ represents the 3-axis steady state wind above the earth's surface and is not modeled in this analysis. From Eq. 54, the perturbed value for ΔV_{TAS} is

$$\Delta V_{TAS} = H_{VA} \Delta \underline{V}_A \tag{57}$$

where

$$H_{VA} = \begin{bmatrix} \frac{u_{Ao}}{V_{TAS_o}} & \frac{v_{Ao}}{V_{TAS_o}} & \frac{w_{Ao}}{V_{TAS_o}} \end{bmatrix} \tag{58}$$

Substituting the perturbed value for $\Delta \underline{V}_A$ obtained from Eq. 56 produces the final expression for ΔV_{TAS},

$$\Delta V_{TAS} = H_{VA} \Delta \underline{v}_B - H_{VA} \Delta \underline{w} \tag{59}$$

The final expressions relating the perturbed values for $\Delta \dot{V}_G$, $\Delta \ddot{h}$, and ΔV_{TAS} and the linear aircraft model are determined by distributing the elements in Eqs. 59, 53, and 40 into Eq. 77 for the chosen order of $\Delta \underline{x}$ and $\Delta \underline{u}$ in Eqs. 78 and 79.

B. GUST MODEL

The gust terms in the model are of a random nature and can be modeled using the well-known Dyrden spectrum, Ref. 10. The modeling effort consists of using spectral factorization methods to obtain a

dynamical system which generates a random process having the specified power spectral density when driven by a white noise process, Ref. 11. Rotational gusts around the aircraft are ignored. The transfer functions for the gusts are as follows,

$$u_g = \sigma_u \left[\frac{L_u}{V_{TAS}}\right]^{\frac{1}{2}} \frac{\sqrt{2}}{\left(1 + \frac{L_u}{V_{TAS}} s\right)} \tag{60}$$

$$v_g = \sigma_v \left[\frac{L_v}{V_{TAS}}\right]^{\frac{1}{2}} \frac{1 + \sqrt{3}\frac{L_v}{V_a} s}{\left(1 + \frac{L_v}{V_{TAS}} s\right)^2} \tag{61}$$

$$w_g = \sigma_w \left[\frac{L_w}{V_{TAS}}\right]^{\frac{1}{2}} \frac{1 + \sqrt{3}\frac{L_w}{V_a} s}{\left(1 + \frac{L_w}{V_{TAS}} s\right)^2} \tag{62}$$

The airspeed, V_{TAS}, is defined in Eq. 54, L_u, L_v, and L_w are the scales of turbulence, and σ_u, σ_v, and σ_w are the variance of the gust. The scales and gust variance are shown in Table 6.

A state-space realization of Eqs. 60 to 62 is

$$\underline{\Delta w} = \begin{bmatrix} \Delta u_g \\ \Delta v_g \\ \Delta w_g \end{bmatrix} = H_w \underline{\Delta w}_g \tag{63}$$

$$\underline{\dot{\Delta w}}_g = A_w \underline{\Delta w}_g + B_w \Delta\eta \tag{64}$$

$$H_w = \begin{bmatrix} 1 & 0 & 0 & 0 & 0 \\ 0 & 1 & 0 & 0 & 0 \\ 0 & 0 & 0 & 1 & 0 \end{bmatrix} \tag{65}$$

$$A_w = \begin{bmatrix} \frac{-V_{TAS_o}}{L_u} & 0 & 0 & 0 & 0 \\ 0 & \frac{-2V_{TAS_o}}{L_v} & 1.0 & 0 & 0 \\ 0 & \frac{-V^2_{TAS_o}}{L^2_v} & 0 & 0 & 0 \\ 0 & 0 & 0 & \frac{-2V_{TAS_o}}{L_w} & 1.0 \\ 0 & 0 & 0 & \frac{-V^2_{TAS_o}}{L^2_w} & 0 \end{bmatrix} \tag{66}$$

$$B_w = \begin{bmatrix} \sigma_u \left[\frac{2V_{A_o}}{L_u}\right]^{1/2} & 0 & 0 \\ 0 & \sigma_v \left[\frac{3V_{A_o}}{L_v}\right]^{1/2} & 0 \\ 0 & \sigma_v \left[\frac{V_{A_o}}{L_v}\right]^{3/2} & 0 \\ 0 & 0 & \sigma_w \left[\frac{3V_{A_o}}{L_w}\right]^{1/2} \\ 0 & 0 & \sigma_w \left[\frac{V_{A_o}}{L_w}\right]^{3/2} \end{bmatrix} \tag{67}$$

$\underline{\eta}$ in Eq. 64 is a 3-vector of independent Gaussian white noise processes with unit variance.

IV. A LINEAR MULTIVARIABLE INNER-LOOP MODEL USEFUL FOR OUTER-LOOP DESIGN

The block diagrams for the inner-loops in Figs. 1, 2, 3, and 4 are relatively straight forward and easily transformed into a nonlinear simulation using the ACSL programming system. Formulating a linear multivariable model for the inner-loop system which is useful for linear simulations and linear analysis is the purpose of this section. The acceleration feedback in the inner-loop complicates the derivation.

Each inner-loop linear model discussed in Chapter II can be placed in the following form

$$\Delta\dot{\underline{x}}_E = E1\Delta\underline{x}_E + E2[\Delta\underline{y}_{IL} + \Delta\underline{v}_{IL}] + E3\Delta\underline{u}_C \tag{68}$$

$$\Delta\delta_{EC} = E4\Delta\underline{x}_E + E5[\Delta\underline{y}_{IL} + \Delta\underline{v}_{IL}] + E6\Delta\underline{u}_C \tag{69}$$

The elevator inner-loop model is used as an example. The other inner-loop linear models representations use A, R, or T in place of E in Eqs. 68 and 69 for aileron, rudder, or throttle inner-loops. The states of the inner-loop dyanmic models shown in Chapter III are as follows

$$\Delta\underline{x}_E^T = [\Delta q_{WO} \quad \Delta\hat{\ddot{h}} \quad \Delta\xi_h] \tag{70}$$

$$\Delta\underline{x}_T^T = [\Delta\hat{\dot{V}}_{CF} \quad \Delta\hat{V}_I \quad \Delta\xi_x \quad \Delta\phi_{WO}] \tag{71}$$

$$\Delta\underline{x}_A^T = [\Delta\hat{p} \quad \Delta\hat{\phi}_C] \tag{72}$$

$$\Delta\underline{x}_R^T = [\Delta r_{WO} \quad \Delta\hat{r}] \tag{73}$$

The vector $\Delta\underline{u}_C$ represents the commands to the inner-loop system

$$\Delta\underline{u}_C^T = [\Delta\ddot{x}_C \quad \Delta\ddot{h}_C \quad \Delta\phi_C \quad \Delta u_C] \tag{74}$$

These commands become the new controls when the inner-loop control system closes the loop around the aircraft dynamics. The vector $\Delta\underline{y}$ represents the inner-loop measurements used for feedback,

$$\Delta\underline{y}^T = [\Delta p \quad \Delta q \quad \Delta r \quad \Delta\phi \quad \Delta V_{GS} \quad \Delta V_{TAS} \quad \Delta\ddot{h}] \tag{75}$$

$$\Delta\underline{a}^T = [\Delta V_{GS} \quad \Delta V_{TAS} \quad \Delta\ddot{h}] \tag{76}$$

The last three inner-loop measurements, $\Delta\underline{a}$, are expressed in terms of the aircraft states, controls, and gust in Chapter III,

$$\Delta\underline{a} = C_a\ \Delta\underline{x} + D_{au}\ \Delta\underline{u} + D_{aw}\ \Delta\underline{w} \tag{77}$$

The vector $\Delta\underline{x}$ represents the states of aircraft, in body axes,

$$\Delta\underline{x}^T = [\Delta u \quad \Delta w \quad \Delta q \quad \Delta\theta \quad \Delta v \quad \Delta p \quad \Delta r \quad \Delta\phi \quad \Delta\psi \quad \Delta x \quad \Delta y \quad \Delta z] \tag{78}$$

The vector, $\Delta\underline{u}$, represents the aircraft controls,

$$\Delta\underline{u}^T = [\Delta\delta_{TH} \quad \Delta\delta_E \quad \Delta\delta_A \quad \Delta\delta_{SPL} \quad \Delta\delta_{SPR} \quad \Delta\delta_R] \tag{79}$$

The vector $\Delta\underline{v}_{IL}$ in Eqs. 68 and 69 are white zero-mean Gaussian noise states representing the measurement noises for the sensors used in the inner-loops. The vector has the following covariance

$$E\{\Delta\underline{v}_{IL}\Delta\underline{v}_{IL}^T\} = \text{DIAGONAL}\ [\sigma^2_{\Delta p}\ \sigma^2_{\Delta q}\ \sigma^2_{\Delta r}\ \sigma^2_{\Delta\phi}\ \sigma^2_{\Delta\dot{V}_{GS}}\ \sigma^2_{\Delta V_{TAS}}\ \sigma^2_{\Delta\ddot{h}}] = V_{IL} \tag{80}$$

The expression $\sigma_{\Delta p}$ is the standard deviation for the measurement noise of the roll rate gyro. The other variables in Eq. 78 are standard

deviations of the measurement noises for the pitch ratio gyro, yaw rate gyro, roll angle from the INS (Inertial Navigation System), inertial along track acceleration from the INS, airspeed sensor, and vertical acceleration from the INS. The actuator command vector, $\Delta\underline{\delta}_c$, is composed of elements from each of the inner-loop control systems discussed in Chapter II,

$$\Delta\underline{\delta}_c^T = [\Delta\delta_{TC}, \Delta\delta_{EC}, \Delta\delta_{AC}, \Delta\delta_{RC}] \tag{81}$$

The model for the linearized actuator dynamics is discussed in Ref. 13, and has the following form,

$$\Delta\underline{u} = F_u \underline{x}_u + G_u \Delta\underline{\delta}_c \tag{82}$$

$$\Delta\dot{\underline{x}}_u = A_u \underline{x}_u + B_u \Delta\underline{\delta}_c \tag{83}$$

In Eq. 79, $\Delta\delta_{TH}$ is thrust while $\Delta\delta_{TC}$ in Eq. 80 is the throttle command.

If all the inner-loop models are combined, the result is as follows,

$$\Delta\dot{\underline{x}}_{IL} = A_{IL}\Delta\underline{x}_{IL} + B_{IY}\,[\Delta\underline{y}_{IL} + \Delta\underline{v}_{IL}] + B_{IC}\Delta\underline{u}_c \tag{84}$$

$$\Delta\underline{\delta}_c = H_{IL}\Delta\underline{x}_{IL} + H_{IY}\,[\Delta\underline{y}_{IL} + \Delta\underline{v}_{IL}] + H_{IC}\Delta\underline{u}_c \tag{85}$$

$$\Delta\underline{y}_{IL} = C_{IL}\Delta\underline{x} + D_{IL}\Delta\underline{u} + D_{IW}\Delta\underline{w}_g \tag{86}$$

Table 7 shows how the matrices in Eqs. 84 to 86 are constructed.

In the rest of the derivation, the inner-loop control system is closed around the aircraft perturbation dyanmics. Substituting Eq. 86 into Eq. 85 and the result into Eq. 81, one obtains

$$\Delta\underline{u} = K_{11}\Delta\underline{x}_p + K_{21}\Delta\underline{u}_c + K_{31}\Delta\underline{v}_{IL} + K_{41}\Delta\underline{u} \tag{87}$$

where

$$\Delta\underline{x}_p^T = [\Delta\underline{x}^T \quad \Delta\underline{w}_g^T \quad \Delta\underline{x}_u^T \quad \Delta\underline{x}_{IL}^T] \tag{88}$$

$$K_{11} = [G_u H_{IY} C_{IL} \quad G_u H_{IY} D_{IW} \quad F_u \quad G_u H_{IL}] \tag{89}$$

$$K_{21} = G_u H_{IC} \tag{90}$$

$$K_{31} = G_u H_{IY} \tag{91}$$

$$K_{41} = G_u H_{IY} D_{IL} \tag{92}$$

Defining

$$Z_u = (I - K_{41})^{-1} \tag{93}$$

Eq. 87 reduces to

$$\Delta\underline{u} = K_1 \Delta\underline{x}_p + K_2 \Delta\underline{u}_c + K_3 \Delta\underline{v}_{IL} \tag{94}$$

where

$$K_1 = Z_u K_{11}, \qquad K_2 = Z_u K_{21}, \qquad K_3 = Z_u K_{31} \tag{95}$$

Rewriting Eq. 86 as

$$\Delta\underline{y}_{IL} = K_{4y} \Delta\underline{x}_p + K_{5y} \Delta u \tag{96}$$

where

$$K_{4y} = [C_{IL} \quad 0 \quad D_{IW} \quad 0] \tag{97}$$

$$K_{5y} = D_{IL}$$

and substituting for $\Delta\underline{u}$ from Eq. 94 results in

$$\Delta \underline{y}_{IL} = K_4 \Delta \underline{x}_p + K_5 \Delta \underline{u}_c + K_6 \Delta \underline{v}_{IL} \tag{99}$$

where

$$K_4 = K_{4y} + K_{5y} K_1 \tag{100}$$

$$K_5 = K_{5y} K_2 \tag{101}$$

$$K_6 = K_{5y} K_3 \tag{102}$$

Substituting Eq. 99 into Eq. 83 and regrouping produces

$$\Delta \dot{\underline{x}}_{IL} = [A_1 + B_{IY} K_4] \Delta \underline{x}_p + [B_{IY} + B_{IY} K_6] \Delta \underline{v}_{IL} + [B_{IC} + B_{IY} K_5] \Delta \underline{u}_c \tag{103}$$

where

$$A_1 = [0 \quad 0 \quad 0 \quad A_{IL}] \tag{104}$$

Substituting Eq. 99 into Eq. 85 produces

$$\Delta \underline{\delta}_c = [H_1 + H_{IY} K_4] \Delta \underline{x}_p + [H_{IY} + H_{IY} K_6] \Delta \underline{v}_{IL} + [H_{IC} + H_{IY} K_5] \Delta \underline{u}_c \tag{105}$$

where

$$H_1 = [0 \quad 0 \quad 0 \quad H_{IL}] \tag{106}$$

Substituting the above into Eq. 82 one obtains

$$\Delta \dot{\underline{x}}_u = [A_2 + B_u [H_1 + H_{IY} K_4]] \Delta \underline{x}_p + B_u [H_{IY} + H_{IY} K_6] \Delta \underline{v}_{IL} + B_u [H_{IC} + H_{IY} K_5] \Delta \underline{u}_c \tag{107}$$

where

$$A_2 = [0 \quad 0 \quad A_u \quad 0] \tag{108}$$

The aircraft dynamics satisfy the equation

$$\Delta\dot{\underline{x}} = A\Delta\underline{x} + B\Delta\underline{u} \tag{109}$$

Substituting Eq. 94 into Eq. 109 produces

$$\Delta\dot{\underline{x}} = [A_3 + BK_1]\Delta\underline{x}_p + BK_3\Delta\underline{v}_{IL} + BK_2\Delta\underline{u}_c \tag{110}$$

where

$$A_3 = [A \quad 0 \quad 0 \quad 0] \tag{111}$$

Combining Eqs. 110, 64, 107, and 103 determines the desired closed-loop model using the inner-loop control system for the linear aircraft dynamics

$$\begin{bmatrix} \Delta\dot{\underline{x}} \\ \Delta\dot{\underline{w}} \\ \Delta\dot{\underline{x}}_u \\ \Delta\dot{\underline{x}}_{IL} \end{bmatrix} = \begin{bmatrix} A_3 + BK_1 & & & \\ 0 & A_w & 0 & 0 \\ A_2 + B_u[H_1 + H_{IY}K_4] & & & \\ A_1 + B_{IY}K_4 & & & \end{bmatrix} \begin{bmatrix} \Delta\underline{x} \\ \Delta\underline{w} \\ \Delta\underline{x}_u \\ \Delta\underline{x}_{IL} \end{bmatrix} + \begin{bmatrix} BK_2 \\ 0 \\ B_u[H_{IC} + H_{IY}K_5] \\ B_{IC} + B_{IY}K_5 \end{bmatrix} \begin{bmatrix} \Delta\underline{u}_c \end{bmatrix}$$

$$+ \begin{bmatrix} BK_3 \\ 0 \\ B_u[H_{IY} + H_{IY}K_6] \\ B_{IY} + B_{IY}K_6 \end{bmatrix} \begin{bmatrix} \Delta\underline{v}_{IL} \end{bmatrix} + \begin{bmatrix} 0 \\ B_w \\ 0 \\ 0 \end{bmatrix} \begin{bmatrix} \Delta\underline{\eta} \end{bmatrix} \tag{112}$$

Equation 112 is the expanded version of Eq. 1 discussed in the introduction.

A. FEATURES OF ACCELERATION FEEDBACK

The Boeing inner-loop control system feeds back the integral of the

acceleration error qunatities

$$e_{\ddot{x}} = \dot{V}_{GS} - \ddot{x}_c \tag{113}$$

and

$$e_{\ddot{h}} = \ddot{h} - \ddot{h}_c \tag{114}$$

to improve stability and tracking. The properties of this type of feedback can be studied by investigating a simple scalar system

$$\dot{x} = ax + bu \tag{115}$$

with the control law

$$u = k_1(\dot{x} - \dot{x}_c) + k_2\,\xi \tag{116}$$

$$\xi = \int(\dot{x} - \dot{x}_c) \tag{117}$$

The closed-loop system for the scalar plant is

$$\begin{bmatrix} \dot{x} \\ \dot{\xi} \end{bmatrix} = \begin{bmatrix} a+b\left(\frac{k_1}{1-k_1b}\right) & \frac{bk_2}{1-k_2b} \\ a+b\left(\frac{k_1}{1-k_1b}\right) & \frac{bk_2}{1-k_2b} \end{bmatrix} \begin{bmatrix} x \\ \xi \end{bmatrix} + \begin{bmatrix} \frac{-bk_1}{1-k_1b} \\ \frac{-bk_1}{1-k_1b} \end{bmatrix} \begin{bmatrix} \dot{x}_c \end{bmatrix} \tag{118}$$

The two rows in the closed-loop plant matrix in Eq. 118 are linearly dependent implying that one of the closed-loop eigenvalues is always zero. Two of the four zero eigenvalues in Table 9 are caused by the way integral feedback is used in the Boeing inner-loop control law.

The steady-state tracking ability of the control law can be investigated using the model

$$\begin{bmatrix} \ddot{x} \\ \xi \end{bmatrix} = \begin{bmatrix} a & 0 \\ 1 & 0 \end{bmatrix} \begin{bmatrix} \dot{x} \\ \xi \end{bmatrix} + \begin{bmatrix} b \\ 0 \end{bmatrix} \dot{u} + \begin{bmatrix} 0 \\ -1 \end{bmatrix} \dot{x}_c \tag{119}$$

when $\dot{x}_c$ is a constant, an expression for $\dot{u}$ can be obtained from Eq. 116. The closed-loop system for Eq. 119 using $\dot{u}$ is

$$\begin{bmatrix} \ddot{x} \\ \dot{\xi} \end{bmatrix} = \begin{bmatrix} a+b\left(\frac{ak_1+k_2}{1-bk_1}\right) & 0 \\ 1 & 0 \end{bmatrix} \begin{bmatrix} \dot{x} \\ \xi \end{bmatrix} + \begin{bmatrix} \frac{-bk_2}{1-bk_1} \\ -1 \end{bmatrix} \dot{x}_c \tag{120}$$

The steady state value for $\dot{x}$ is given by

$$\dot{x} = \frac{bk_2}{a+bk_2} \dot{x}_c \tag{121}$$

Unless a is zero, there is no value for k_2 which makes $\dot{x}$ equal to $\dot{x}_c$ in steady state. A step command for $\Delta\ddot{h}_c$ in Chapter IV shows that perfect steady state tracking is not obtained in simulation even though integral feedback is employed in the Boeing inner-loop control system.

V. INNER-LOOP MODEL VERFICATION

The purpose of this chapter is to compare time histories between the linear inner-loop closed-loop models and the nonlinear ACSL simulation model which includes nonlinear models of the inner-loops control systems. A number of options are available when the linear model is constructed. Table 8 shows the options and the recommended settings currently employed.

The effect of varying the engine dynamics EPR time constant is investigated in the longitudinal dynamics verification. The effects of the lead/lag filter and spoiler aerodynamics are investigaged in the lateral-directional dyanmics verification. The choice of the first two options shown in Table 8, remain unresolved.

A. LONGITUDINAL

The simulation comparison has two purposes. The first purpose is computer coding verification. The second purpose is to identify nonlinearities which cause a significant descrepancy between linear and nonlinear dynamics.

The autothrottle has a significant nonlinearity in the upper and lower saturation limits for the rate of change of EPR (engine pressure ratio) as discussed in Ref. 12. The effect of the saturation limit is to decrease the EPR dynamics time constant in a manner similiar to Eq. 18. Unsaturated, the EPR dynamics time constant is -0.2 sec. A time constant of -2.0 sec is used in Ref. 12. Figure 6 shows the effect of τ_{EPR} for

-0.2, -0.5, and -2.0. The simulation comparisons in Fig. 6 are in good agreement. The recommended τ_{EPR} is -0.2, i.e., no saturation effect is needed in the linear model.

Originally there were significant mismatch between linear and nonlinear autothrottle simulations. The mismatch was traced to a subtle error in the calculation of the upper saturation limit of EPR in the ACSL nonlinear simulation, which was subsequently corrected. The error in the ACSL program existed, but apparantly did not affect the results in Ref. 12.

The time history comparisons for a $\Delta\ddot{h}_c$ command is shown in Fig. 7 and has excellent agreement. The Δh response is also shown in Fig. 7 and as discussed in Chapter III, the steady state error is not zero even though the inner-loop control system feeds back the integral of the command error.

The inner-loop closed-loop eigenvalues for the longitudinal system are shown in Table 9. The phugoid mode and the short period are stable and well damped. The effect of changing τ_{EPR} has almost no effect on the eigenvalues. Residualizing the elevator actuator dynamics primarily affects the eigenvalue for the $\Delta\ddot{h}$ filter by further stabilizing its value. The two zero eigenvalues for $\Delta\xi_x$ and $\Delta\xi_h$ are a feature of feeding back the integral of acceleration as discussed in Chapter III. The states associated with the gust model (Δw_{g1}, Δw_{g2}, and Δw_{g3}) and the wind shear estimator ($\Delta\hat{\dot{V}}_{cf}$ and $\Delta\hat{\dot{V}}_I$) are uncontrollable and have eigenvalues which remain fixed for variations in the aircraft dynamics.

B. LATERAL-DIRECTIONAL

The largest discrepancy between linear and nonlinear models occurs

for the aileron inner-loop control system. The discrepancy is caused by the highly nonlinear aileron/spoiler actuator system discussed in Ref. 12. The linear model for the inner-loop control system and actuator is constructed so that any subset of the nonlinearities can be represented in the model.

Three linear models are simulated for step $\Delta\phi_c$ commands of 2.0 deg and are shown in Fig. 8. The roll command is large enough so that spoiler is activated when $\Delta\phi_c$ = 2.0 deg, but when $\Delta\phi_c$ returns to zero, little spoiler is used. The assumptions in constructing the three linear models are discussed in Table 10, which shows the closed-loop eigenvalues.

The closed-loop eigenvalues indicate that the Dutch Roll mode, spiral mode, and roll mode are very stable. In CASE 1, the slow actuator eigenvalue, -0.975, is deceptive since it can be shown that the eigenvalue is almost cancelled by a zero of nearly equal value. The aileron actuator in CASE 1 responds almsot immediately to the commanded aileron value as long as the value has a finite rate. The simulations in Ref. 12 for step ($\approx$ infinite rate) commands in the aileron actuator can be misleading in this regard.

CASE 2 models the aileron actuator as it existed before many of the mechanical nonlinearities were added. The fast aileron actuator mode forms a complex pair with the yaw rate filter mode. The roll mode becomes more stable.

CASE 3 includes the effect of spoiler. In the nonlinear model, spoiler is activated after the aileron actuator surface commands exceeds certain values ($\approx$ 2.2 deg). Including the effect of spoiler when $\Delta\phi_c$ is small produces incorrect results. Not including spoiler when $\Delta\phi_c$ is of moderate value may not produce correct results.

The simulations in Fig. 8 show that CASE 1 and 2 match the nonlinear simulation for small $\Delta\phi_c$ commands. Using a $\Delta\phi_c$ of -25 degs and Eq. 18, Fig. 9 shows the descrepancies that occur as $\Delta\phi_c$ is increased. The effect of the saturation limit in reducing the roll response rate limit for large roll commands is clearly evident in Fig. 9. The roll command saturation limits are apparantly not used in the simulations in Ref. 6 where -25 deg roll commands are used to test for limit cycles.

Rudder commands of 2.0 deg are simulated in Fig. 10 for two cases. The rudder linear and nonlinear response match well. Continued problems with the linear model for the aileron/spoiler actuator system is evident in the aileron response in Fig. 10. Including spoiler feedback increases the aileron command control effectiveness.

VI. SUMMARY

The linear and nonlinear inner-loop control system models to be used in a 3-D R/NAV outer-loop control synthesis problem are presented in this report. Most of the modes with fast eigenvalues are retained in the linear model since they do not pose a problem to the outer-loop (limited state feedback) control synthesis procedure. Closed-loop eigenvalues for the inner-loop control system discussed in the report show that all inner-loop complex modes are well damped and inner-loop real modes are acceptably stable.

Small step commands in each of the outer-loop control variables show good agreement between linear and nonlinear model time histories. The roll inner-loop control system is identified as the model with the most descrepancy primarily because of the highly nonlinear aileron/spoiler actuator.

REFERENCES

1. Halyo, Nesim, "Development of an Advanced 3D Guidance and Control Law for Curved Path Tracking", ICS Technical Proposal, September 1978.

2. Boeing Document D6-32669, "Flight Critical Control Laws for the NASA Terminal Controlled Vehicle," September 1975.

3. Boeing Document D6-41565, "Guidance Algorithms and Non-Critical Control Laws for ADEDS and the AGCS", May 1974.

4. Boeing Document D6-32686-1 "Terminal Configured Vehicle (TCV) B-737 Navigation Computer Software Description", NASA Langley, Hampton, VA August, 1978.

5. Boeing Document D6-34279, "NASA 515 Flight Control System Description-RSFS Aircraft", September 1976.

6. Boeing Document D6-42695, " NASA 515 Roll Attitude Loop Stability Investigations", February 1976.

7. Margolis, S. P., Wolverton, D. A., Hamm, R. W., "Flight Control Computer Software Descriptions", CSC Number 33509, Computer Sciences Corporation, Hampton, VA, July 1979.

8. Broussard, J. R, and Glasson, D. P., "Optimal Multirate Flight Control System Design", JACC, San Francisco, August 1980.

9. Broussard, J. R., "Design, Implementation and Flight Testing of PIF Autopilot Designs for General Aviation Aircraft", Information & Control Systems, Inc., Report No. 681102, October 1981.

10. Martin, D. J., "Real-Time Simulation of Atmospheric Turbulence", Masters Thesis, The George Washington University, May 1979.

11. Halyo, Nesim, "Development of a Digital Guidance and Control Law for Steep Approach Automatic Landings Using Modern Control Techniques", NASA CR-3074, February 1979.

12. Broussard, J. R., and Stallman, S. T., "Modification and Verification of an ACSL Simulation of the ATOPS B-737 Research Aircraft", NASA CR-166049, February 1983.

APPENDIX A

Recently, an alternative FORTRAN simulation of the ATOPS B-737 aircraft was made available to ICS by NASA. As part of the verification of the new simulation, inner-loop step commands time histories computed using the ACSL simulation were similarily computed using the FORTRAN simulation. The descrepancies between the simulations were identified and partially eliminated. Figures 11 to 14 show the comparisons for the same step commands made in Figs. 6, 7, 8 and 10. The most notable difference is for the autothrottle control system in Fig. 11. The aileron response difference in Fig. 13 is caused by the fact that the FORTRAN simulation at the time the simulation was performed did not include the lead/lag compensator and did have spoiler feedback. In Fig. 14, the FORTRAN simulation included the lead/lag compensator and spoiler feedback and the aileron responses are in reasonable agreement.

TABLE 1. AUTOTHROTTLE BLOCK DIAGRAM GAIN VALUES

GAIN	VALUE
k_1	5.0
k_2	16.0
k_3	0.3
k_4	1.0
k_5	10.0
k_6	2.0
k_7	1.5
k_8	60.0
k_9	1.2
k_{10}	5.0
k_{11}	1.0
k_{12}	0.2
k_{13}	16.0

TABLE 2. ELEVATOR BLOCK DIAGRAM GAIN VALUES

GAIN	VALUE
k_{14}	296.5
k_{15}	1.0
k_{16}	0.275
k_{17}	120.0
k_{18}	360.0
k_{19}	20.0
k_{20}	0.1
k_{21}	5.0
k_{22}	4.0
k_{23}	80.0
k_{24}	0.25
k_{25}	0.25
k_{26}	0.004
k_{27}	2.16
k_{28}	16.0
k_{29}	10.0
k_{30}	62.4

TABLE 3. AILERON/SPOILER BLOCK DIAGRAM GAIN VALUES

GAIN	VALUE
k_{31}	20.0
k_{32}	0.05
k_{33}	1.4
k_{34}	50.0
k_{35}	25.0
k_{36}	5.0
k_{37}	4.0
k_{38}	2.0
k_{39}	97.66

TABLE 4. RUDDER BLOCK DIAGRAM GAIN VALUES

GAIN	VALUE
k_{40}	2.31
k_{41}	0.143
k_{42}	3.33
k_{43}	1.0
k_{44}	4.0

TABLE 5 BREAKPOINTS FOR YAW DAMPER GAIN VERSUS AIRSPEED

INPUT	CAS (kts)	100.00	122.4	150.0	206.0	450.0
OUTPUT	KYD	1.0	0.765	0.61	0.395	0.31

TABLE 6 SCALES AND VARIANCE FOR GUST MODELS

	ALTITUDE h (ft)	0-60	60-328	328-1750	>1750
σ_u (ft/sec)		16.0	$60.72h^{-0.32}$	10.0	10.0
σ_v (ft/sec)		12.7	$26.50h^{-0.18}$	10.0	10.0
σ_w (ft/sec)		9.3	9.3	9.3	9.3
L_u (ft)		560.0	560.0	$10.85h^{0.68}$	1750.0
L_v (ft)		320.0	$102.17h^{0.28}$	$10.02h^{0.68}$	1750.0
L_w (ft)		174.0	$12.65h^{0.64}$	$10.02h^{0.68}$	1750.0

$$A_{IL} = \begin{bmatrix} T1 & 0 & 0 & 0 \\ 0 & E1 & 0 & 0 \\ 0 & 0 & A1 & 0 \\ 0 & 0 & 0 & R1 \end{bmatrix} \qquad B_{IY} = \begin{bmatrix} T2 \\ E2 \\ A2 \\ R2 \end{bmatrix}$$

$$B_{IC} = \begin{bmatrix} T3 \\ E3 \\ A3 \\ R3 \end{bmatrix} \qquad H_{IL} = \begin{bmatrix} T4 & 0 & 0 & 0 \\ 0 & E4 & 0 & 0 \\ 0 & 0 & A4 & 0 \\ 0 & 0 & 0 & R4 \end{bmatrix}$$

$$H_{IY} = \begin{bmatrix} T5 \\ E5 \\ A5 \\ R5 \end{bmatrix} \qquad H_{IC} = \begin{bmatrix} T6 \\ E6 \\ A6 \\ R6 \end{bmatrix}$$

$$C_{IL} = \begin{bmatrix} 0 & 0 & 0 & 0 & 0 & 1 & 0 & 0 & 0 & 0 & 0 & 0 \\ 0 & 0 & 1 & 0 & 0 & 0 & 0 & 0 & 0 & 0 & 0 & 0 \\ 0 & 0 & 0 & 0 & 0 & 0 & 1 & 0 & 0 & 0 & 0 & 0 \\ 0 & 0 & 0 & 0 & 0 & 0 & 0 & 1 & 0 & 0 & 0 & 0 \\ & & & & & & C_a & & & & & \end{bmatrix}$$

$$D_{IL} = \begin{bmatrix} 0 \\ D_{au} \end{bmatrix} \qquad D_{IW} = \begin{bmatrix} 0 \\ D_{aw} \end{bmatrix}$$

TABLE 7. INNER-LOOP CONTROL SYSTEM MATRICES

OPTIONS	RECOMMENDED VALUE
INCLUDE SPOILER FEEDBACK	CURRENTLY OPTIMAL
INCLUDE LEAD/LAG DYNAMICS	CURRENTLY OPTIMAL
ENGINE EPR TIME CONSTANT	-0.2 SEC
RESIDUALIZE SPOILER ACTUATOR STATE	TRUE
INCLUDE EFFECTS OF PCU RATE LIMITS	FALSE
INCLUDE EFFECTS OF BACKLASH IN AILERON ACTUATOR MODEL	FALSE
RESIDUALIZE RUDDER ACTUATOR STATE	TRUE
RESIDUALIZE ELEVATOR ACTUATOR STATE	FALSE
INCLUDE EFFECT OF EPR REDUCTION IN CHOOSING Y IN EQ. 11	FALSE, Y = 1.0
RESIDUALIZE $\Delta\hat{p}$ STATE	FALSE
RESIDUALIZE $\Delta\hat{\dot{x}}$ STATE	FALSE
RESIDUALIZE $\Delta\hat{r}$ STATE	FALSE
INCLUDE SATURATION DESCRIBING FUNCTION FACTOR IN $\Delta\phi_c$	FALSE
INCLUDE SATURATION DESCRIBING FUNCTION FACTOR IN $\Delta\ddot{x}_c$	FALSE
INCLUDE SATURATION DESCRIBING FUNCTION FACTOR IN $\Delta\ddot{h}_c$	FALSE

TABLE 8 OPTIONS IN CONSTRUCTING THE INNER-LOOP MODEL

CASE	τ_{EPR}=-0.2	τ_{EPR}=-0.5	EPR=-0.5,$\Delta\delta e$ ACTUATOR STATE RESIDUALIZED	τ_{EPR}=-2.0
Δx	0.0	0.0	0.0	0.0
Δz	0.0	0.0	0.0	0.0
$\Delta\xi_x$	0.0	0.0	0.0	0.0
$\Delta\xi_h$	0.0	0.0	0.0	0.0
PHUGOID MODE	-0.057±j0.03 ω_n=0.065,ξ=0.878	-0.057±j0.03 ω_n=0.065,ξ=0.878	-0.057±j0.03 ω_n=0.065,ξ=0.878	-0.058±j0.03 ω_n=0.066,ξ=0.878
$\Delta\omega_{g1}$	-0.138	-0.138	-0.138	-0.138
$\Delta\omega_{g2}$	-0.149	-0.149	-0.149	-0.149
$\Delta\omega_{g3}$	-0.149	-0.149	-0.149	-0.149
$\Delta\hat{\dot{V}}_{cf}$	-0.20	-0.20	-0.20	-0.20
$\Delta\hat{q}_{wo}$	-0.242	-0.254	-0.254	-0.335 j0.155*
Δx_{EPR}	-5.53	-2.11	-2.11	ω_n=0.369, =0.907*
SHORT PERIOD MODE	-1.77±j1.93 ω_n=2.62,ξ=0.675	-1.77±j1.94 ω_n=2.63,ξ=0.673	-1.78±j1.86 ω_n=2.60,ξ=0.693	-1.76±j1.94 ω_n=2.62,ξ=0.675
$\Delta\hat{V}_I$	-5.0	-5.0	-5.0	-5.0
$\Delta\hat{\dot{h}}$	-7.39	-7.39	-8.49	-7.39
$\Delta\delta_e$	-23.5	-23.5	---	-23.5

* Two Reals Formed a Complex Pair

TABLE 9 INNER-LOOP LOGTITUDINAL CLOSED-LOOP EIGENVALUES

CASE	1	2	3
Δy	0.0	0.0	0.0
$\Delta\psi$	0.0	0.0	0.0
Δw_{g1}	-0.149	-0.149	-0.149
Δw_{g2}	-0.149	-0.149	-0.149
Δr_{wo}	-0.273	-0.275	-0.397
$\Delta\delta_a$	-0.975	-6.09±j2.13*	-0.975
DUTCH ROLL MODE	-0.875±j0.605	-0.902±j0.574	-1.01±j0.24
	ω_n=1.06,ξ=0.822	ω_n=1.07,ξ=0.843	ω_n=1.04,ξ=0.973
SPRIAL MODE	-1.6	-1.6	-1.6
ROLL MODE	-2.73	-3.56	-4.58
ROLL COMMAND	-5.0	-5.00	-5.0
$\Delta\dot{r}$	-5.85	ω_n=6.45,ξ=0.943*	-10.5±j5.0*
$\Delta\dot{p}$	-17.4	-22.5	ω_n=11.6,ξ=0.903*

* Reals Combined to Form a Complex Pair

TABLE 10 INNER-LOOP LATERAL/DIRECTIONAL CLOSED-LOOP EIGENVALUES

CASE 1

NO SPOILER AERODYNAMIC EFFECT IN B MATRIX, LEADLAG COMPENSATOR DYNAMICS INCLUDED IN A MATRIX

CASE 2

NO SPOILER AERODYNAMIC EFFECT IN B MATRIX, LEADLAG COMPENSATOR DYNAMICS NOT INCLUDED IN A MATRIX

CASE 3

SPOILER AERODYNAMIC EFFECT IN B MATRIX, SPOILER ACTUATOR STATE IS RESIDUALIZED, LEADLAG COMPENSATOR DYNAMICS INCLUDED IN A MATRIX

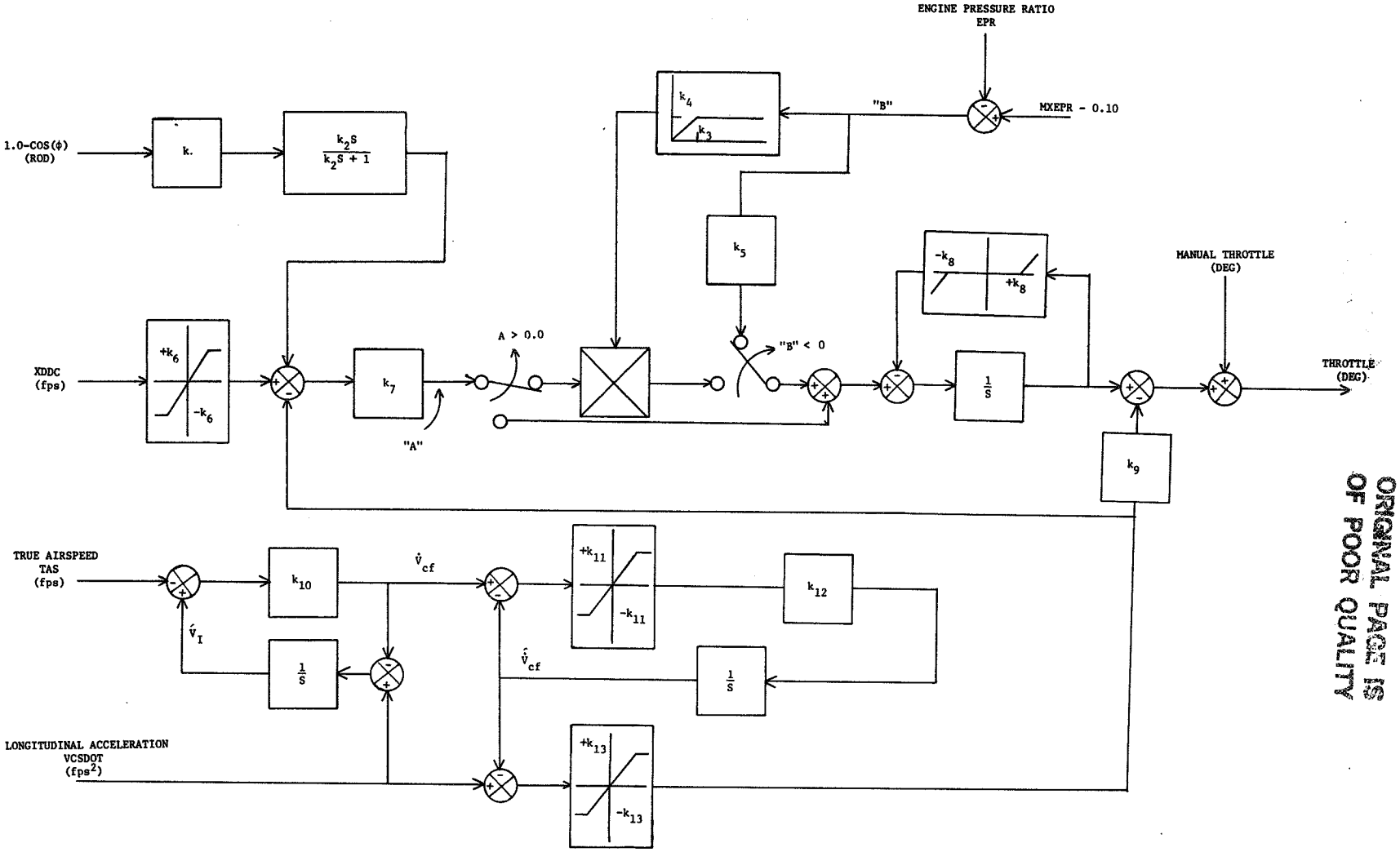

FIGURE 1 AUTOTHROTTLE INNER-LOOP CONTROL SYSTEM BLOCK DAGRAM

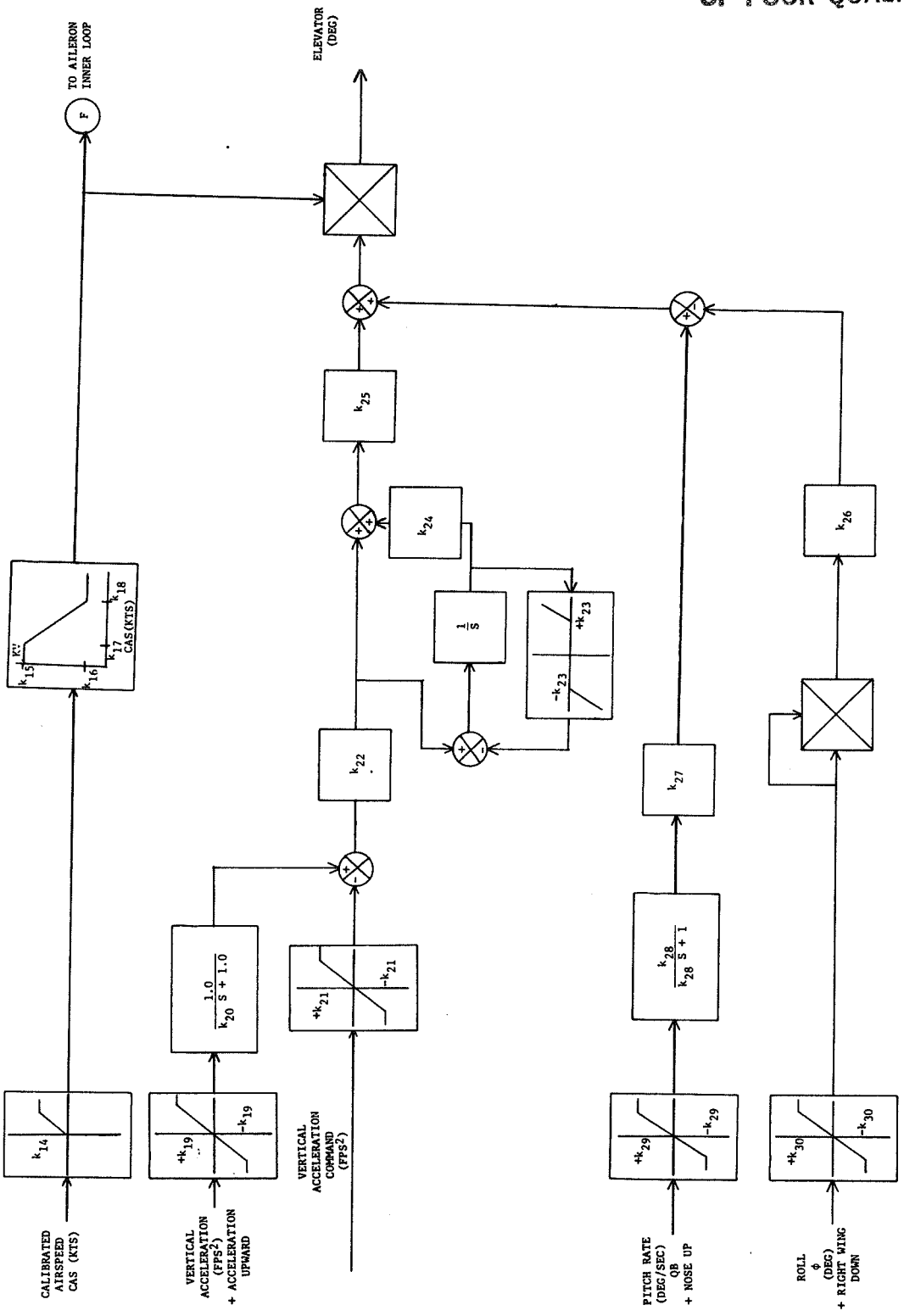

FIGURE 2 ELEVATOR INNER-LOOP CONTROL SYSTEM DIAGRAM

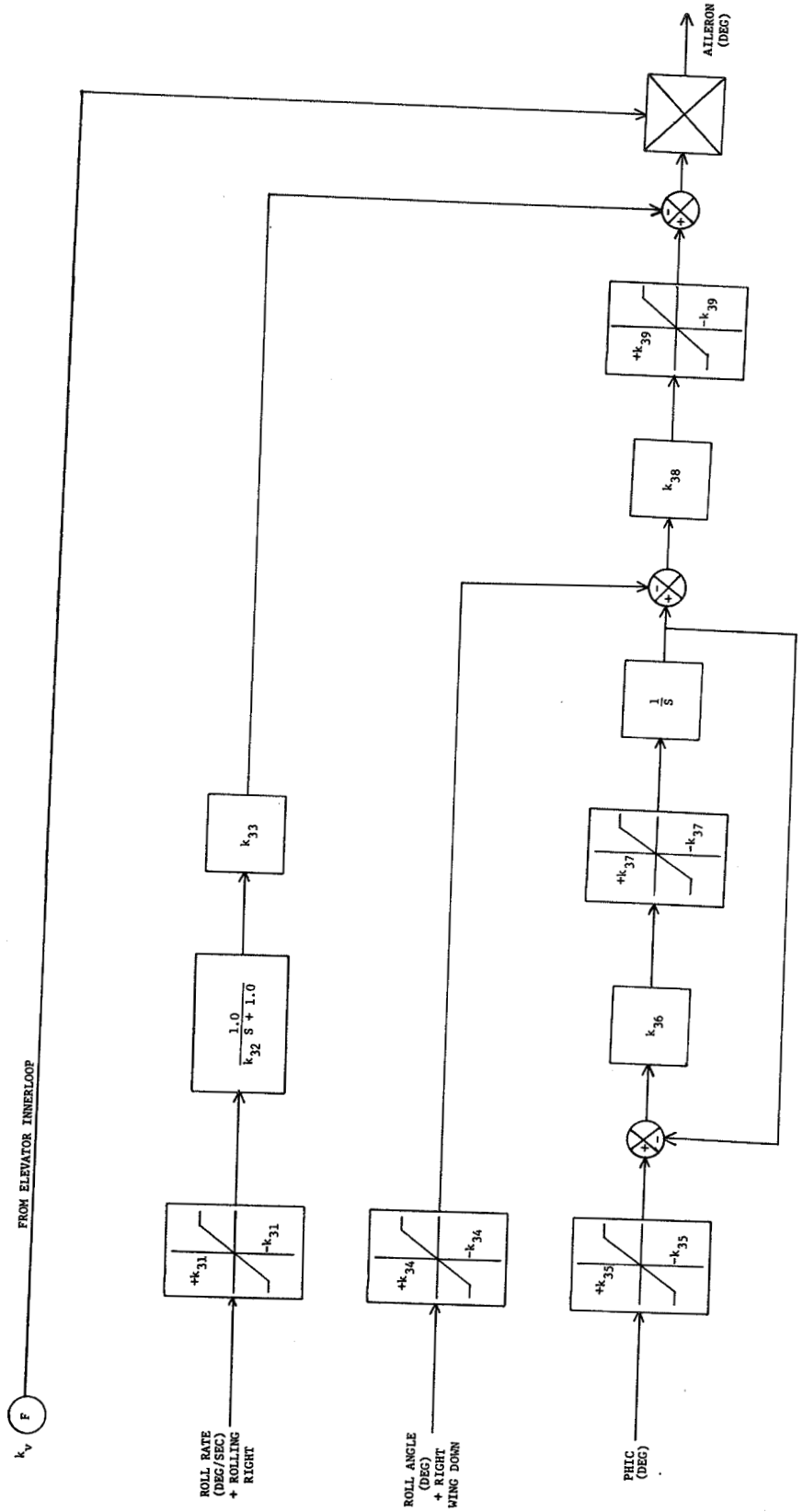

FIGURE 3 AILERON/SPOILER INNER-LOOP CONTROL SYSTEM BLOCK DIAGRAM

FIGURE 4 YAW DAMPER AND RUDDER ACTUATOR MODEL DIAGRAM

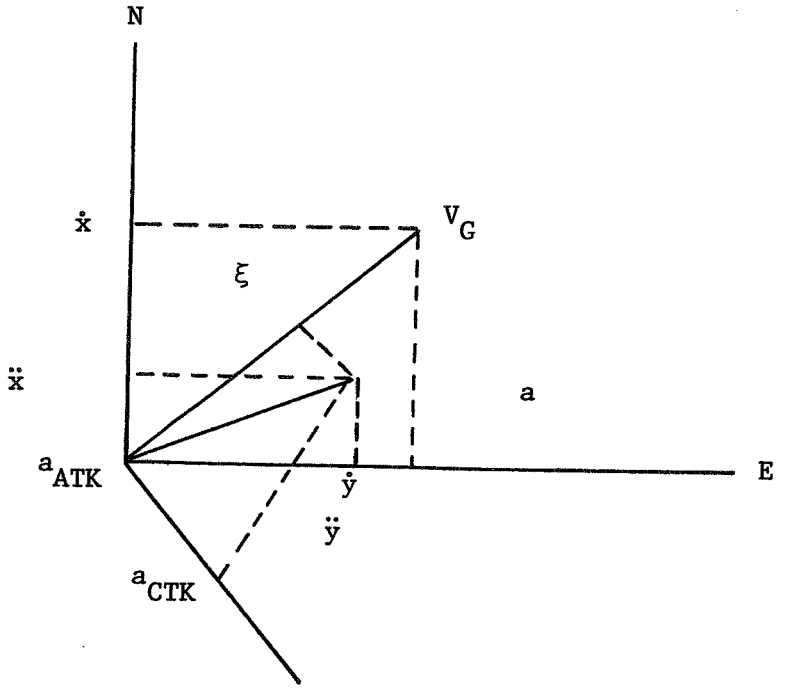

FIGURE 5 LOCAL LEVEL VECTOR DIAGRAM

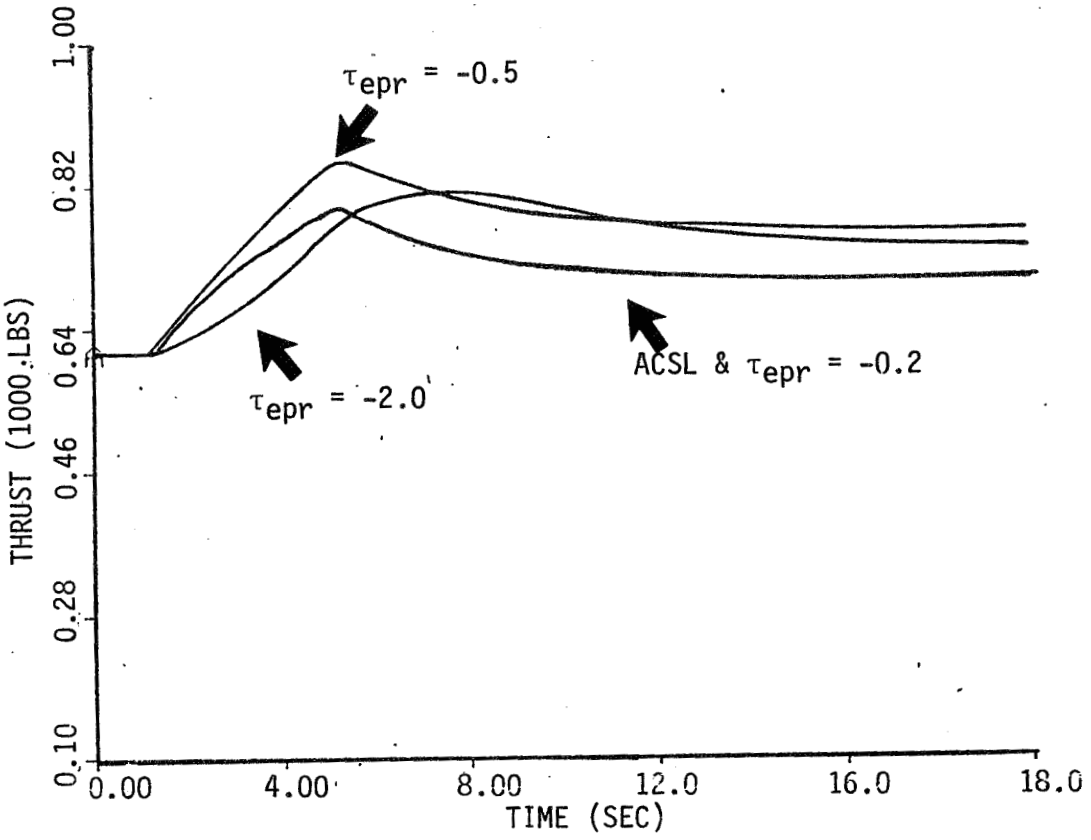

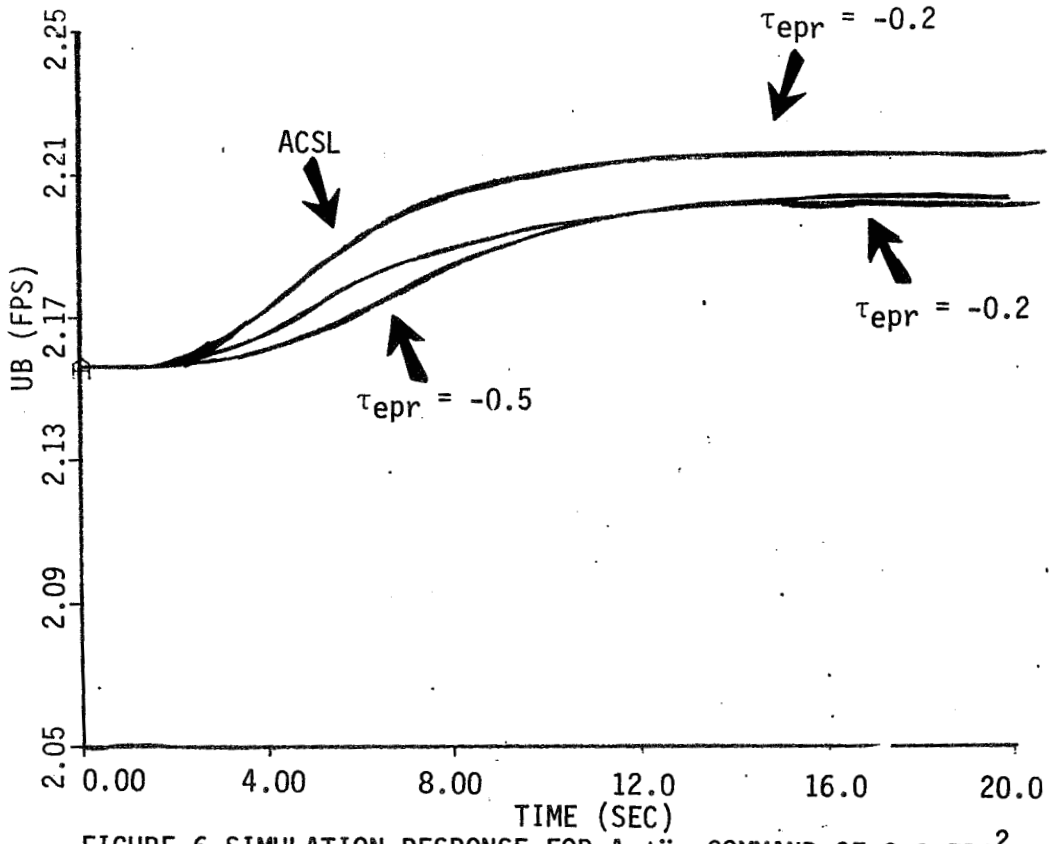

FIGURE 6 SIMULATION RESPONSE FOR A $\Delta\ddot{x}_c$ COMMAND OF 2.0 FPS^2.

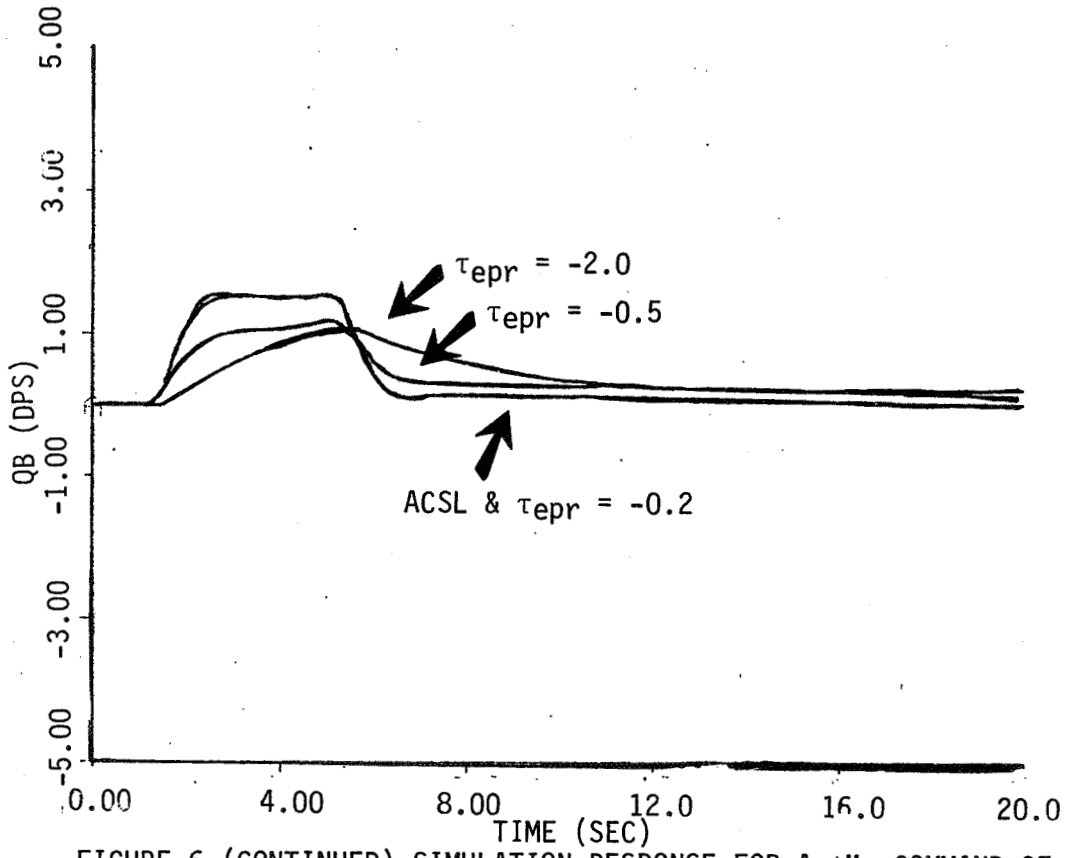

FIGURE 6 (CONTINUED) SIMULATION RESPONSE FOR A $\Delta\ddot{x}_c$ COMMAND OF 2.0 FPS^2.

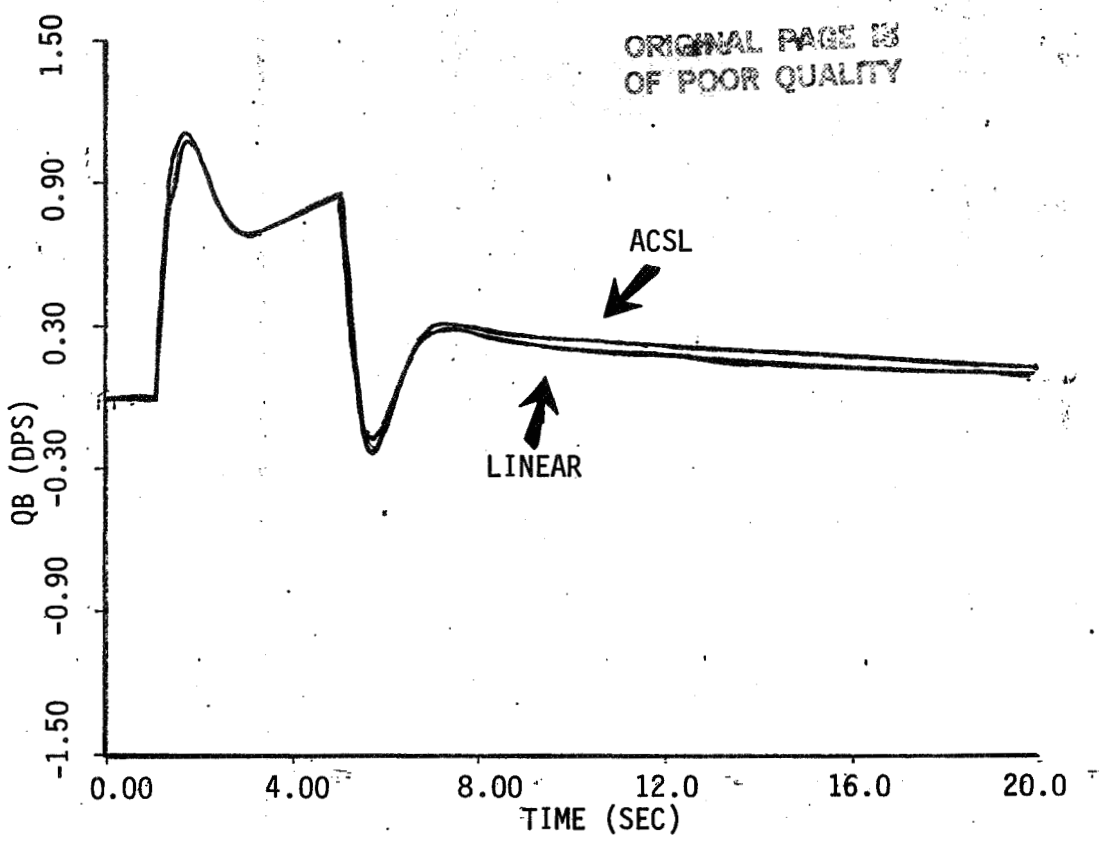

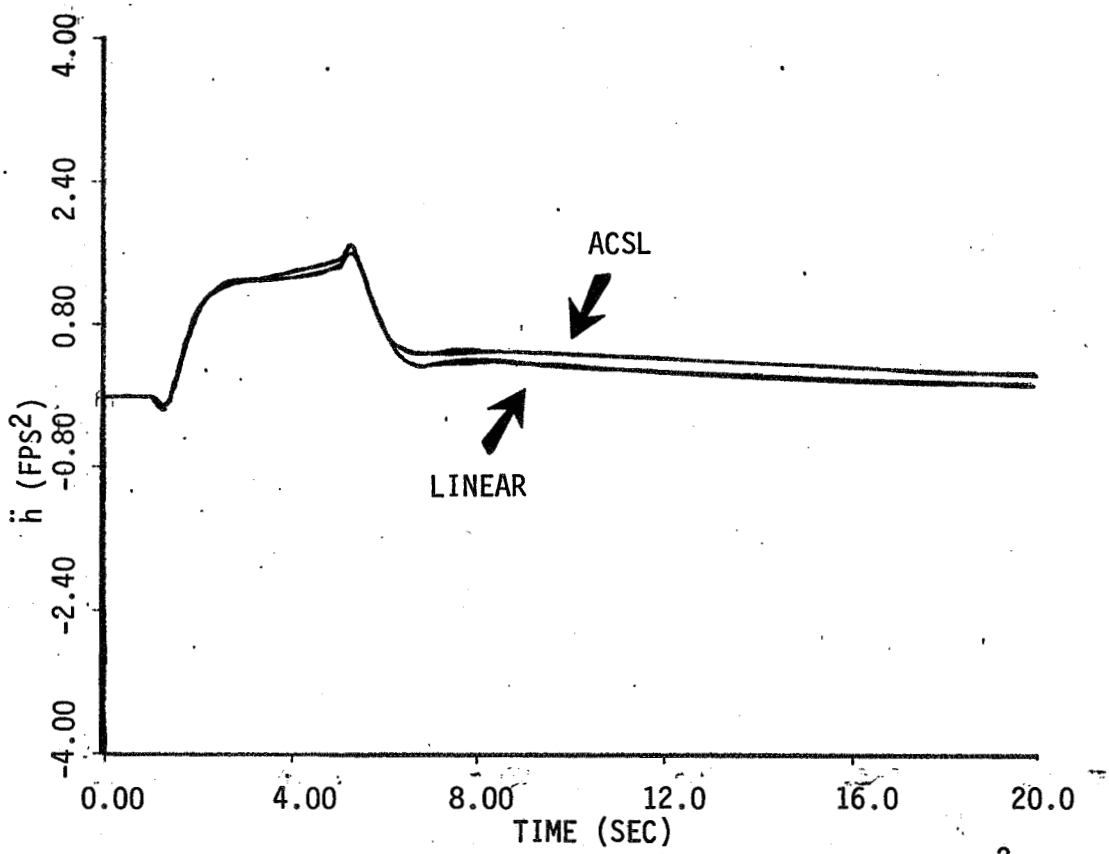

FIGURE 7 SIMULATION RESPONSE FOR A $\Delta\ddot{h}_c$ COMMAND OF 2.0 FPS^2.

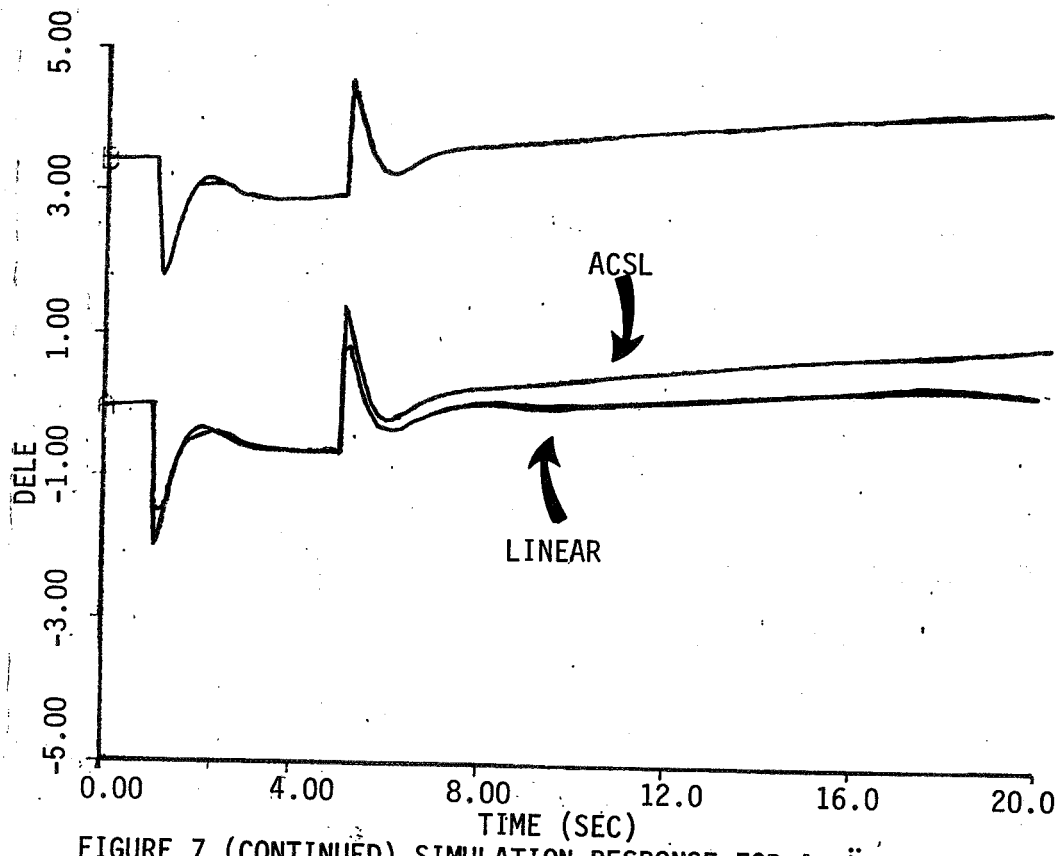

FIGURE 7 (CONTINUED) SIMULATION RESPONSE FOR A $\Delta\ddot{h}_c$ COMMAND OF 2.0 FPS^2.

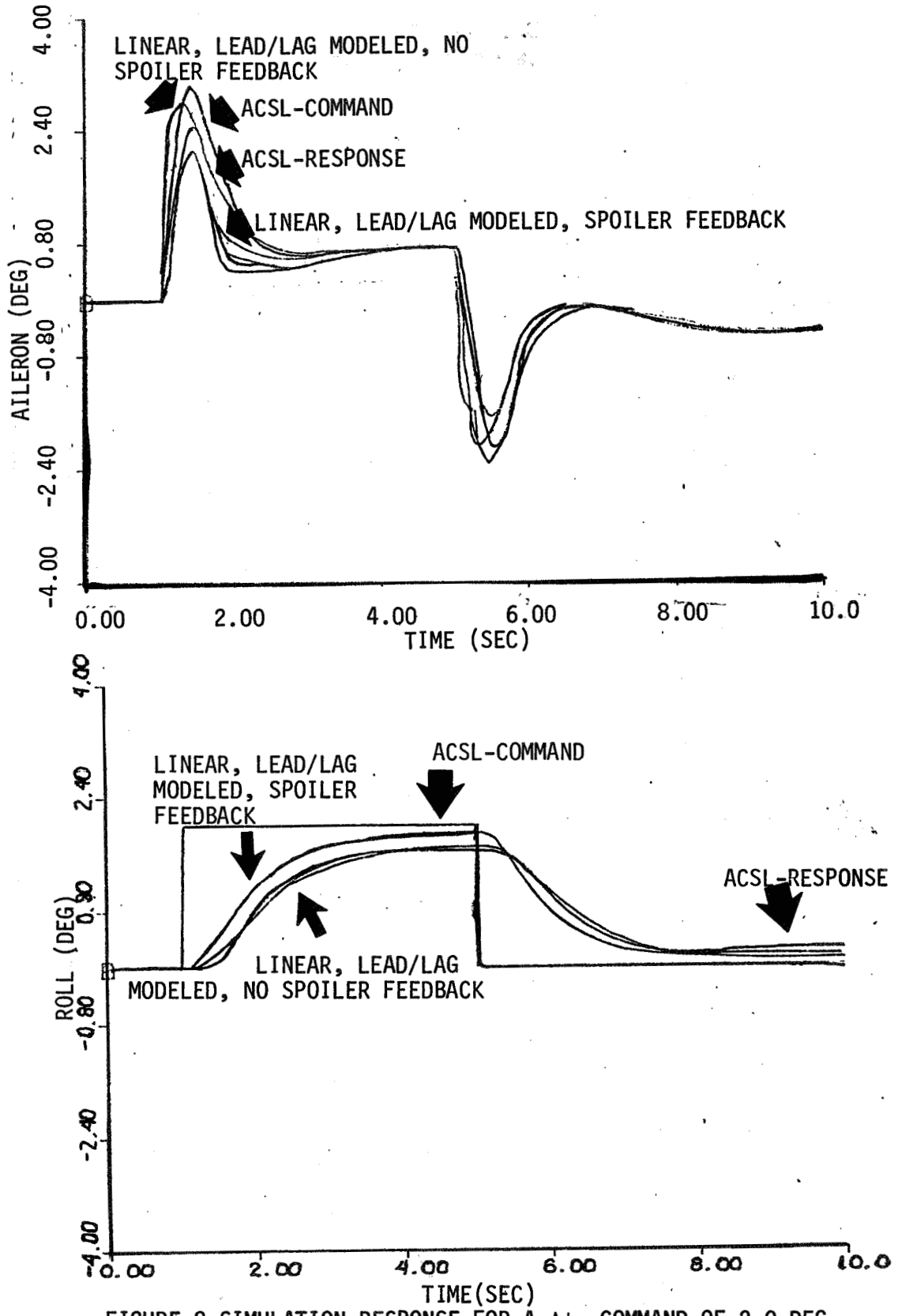

FIGURE 8 SIMULATION RESPONSE FOR A $\Delta\phi_C$ COMMAND OF 2.0 DEG.

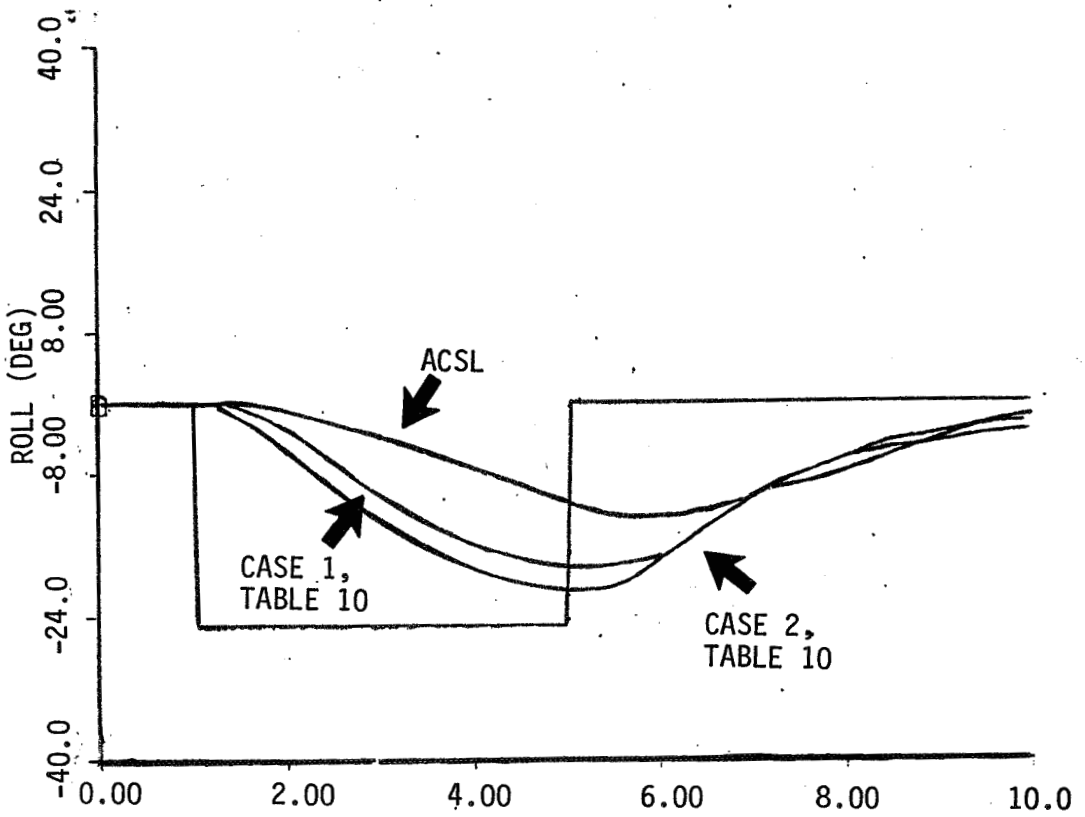

FIGURE 9 SIMULATION RESPONSE FOR A $\Delta\phi_C$ COMMAND OF -25.0 DEG.

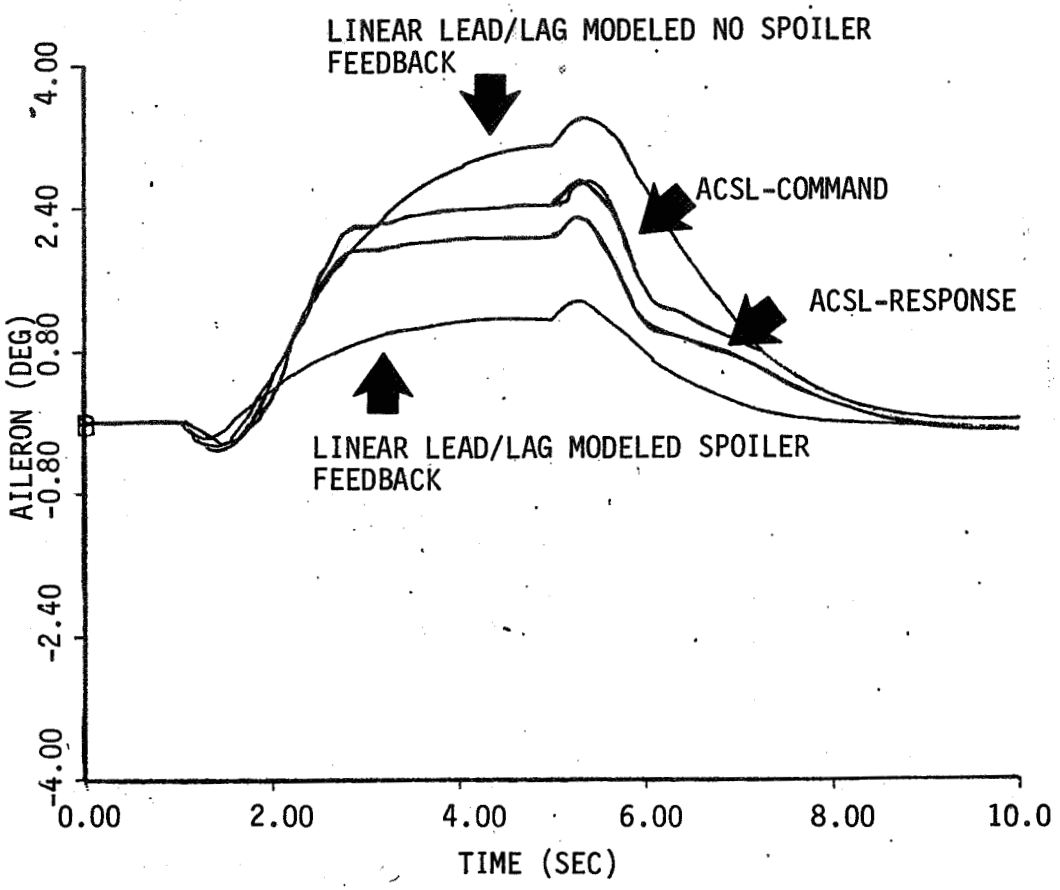

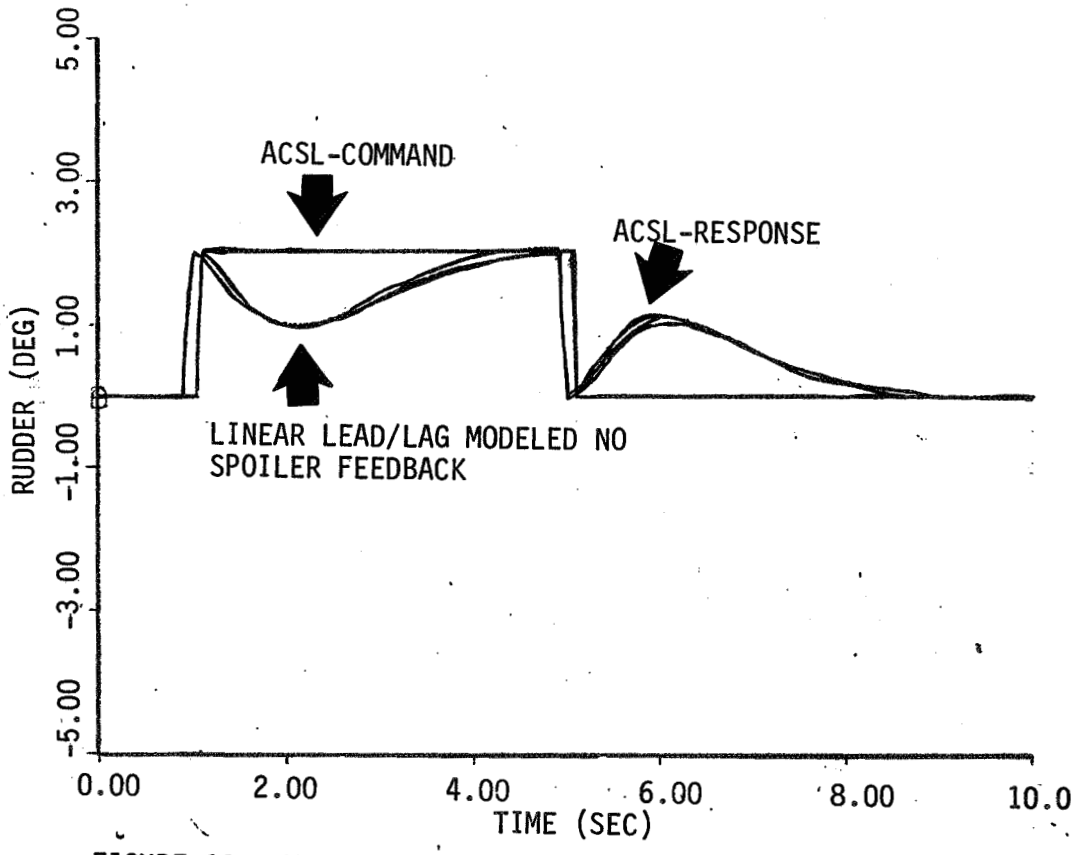

FIGURE 10 SIMULATION RESPONSE FOR A U_C COMMAND OF 2.0 DEG.

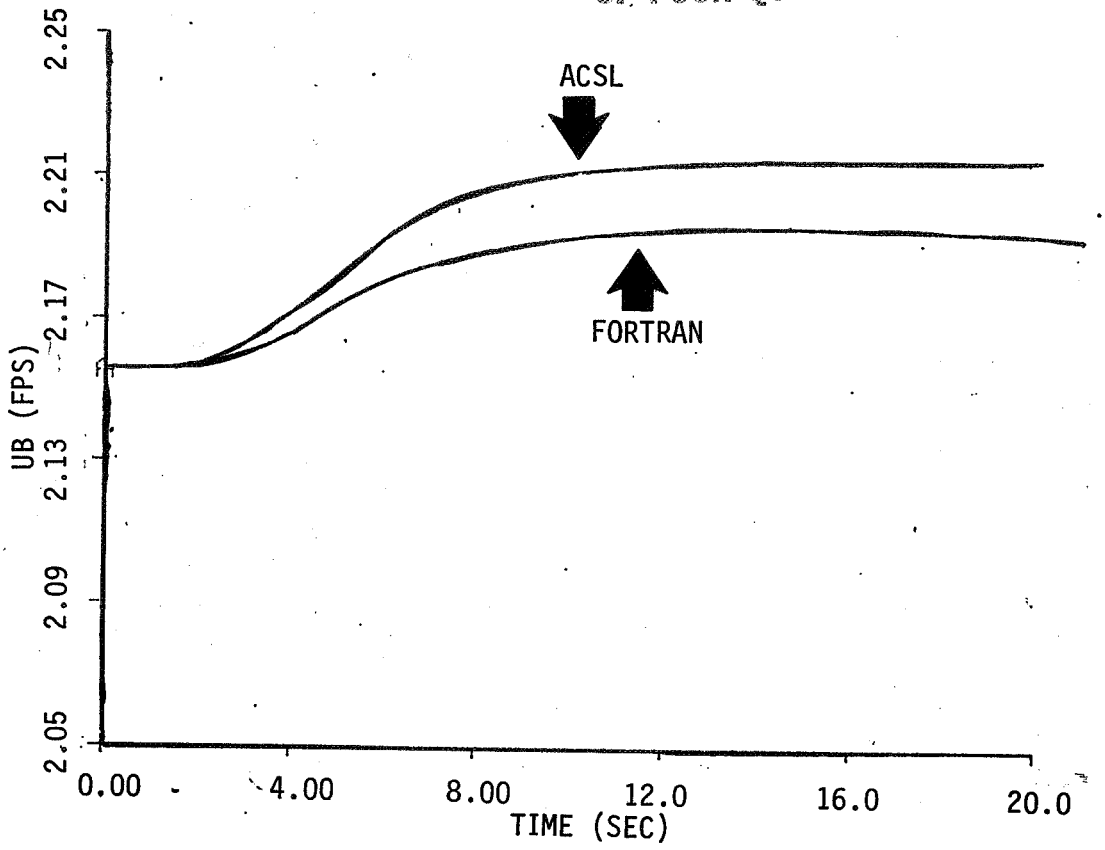

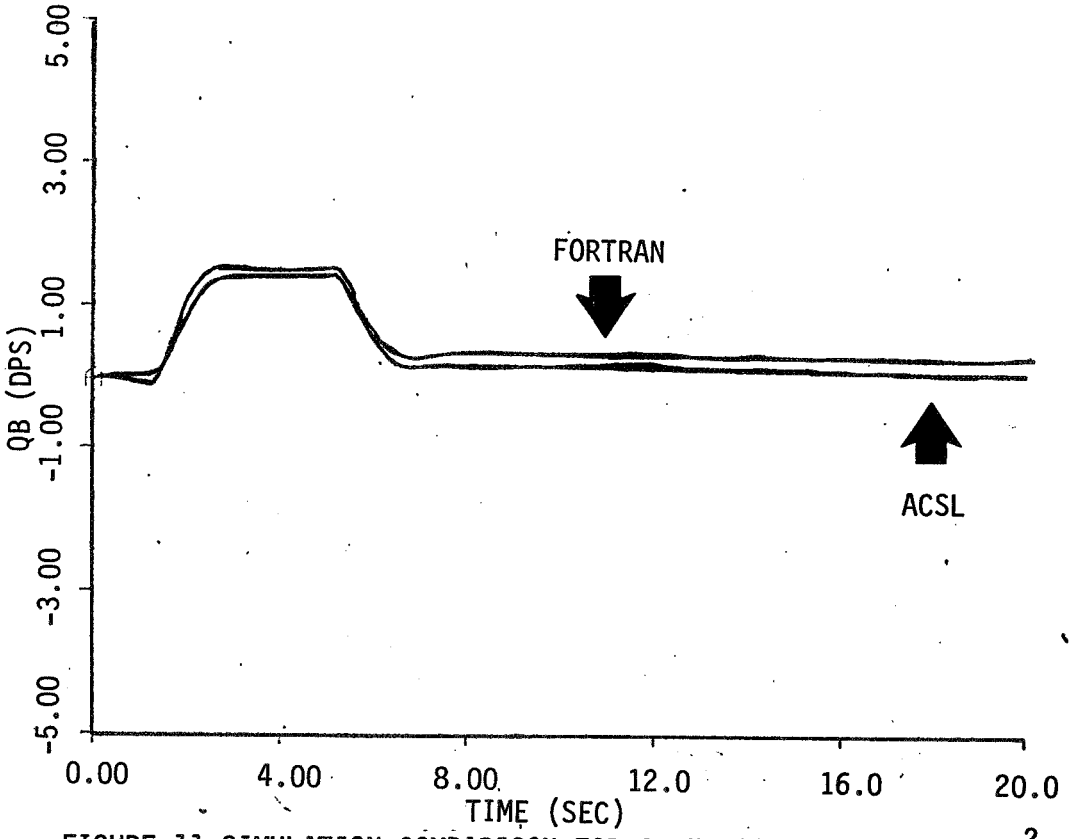

FIGURE 11 SIMULATION COMPARISON FOR A $\Delta\ddot{x}_c$ COMMAND OF 2.0 FPS^2.

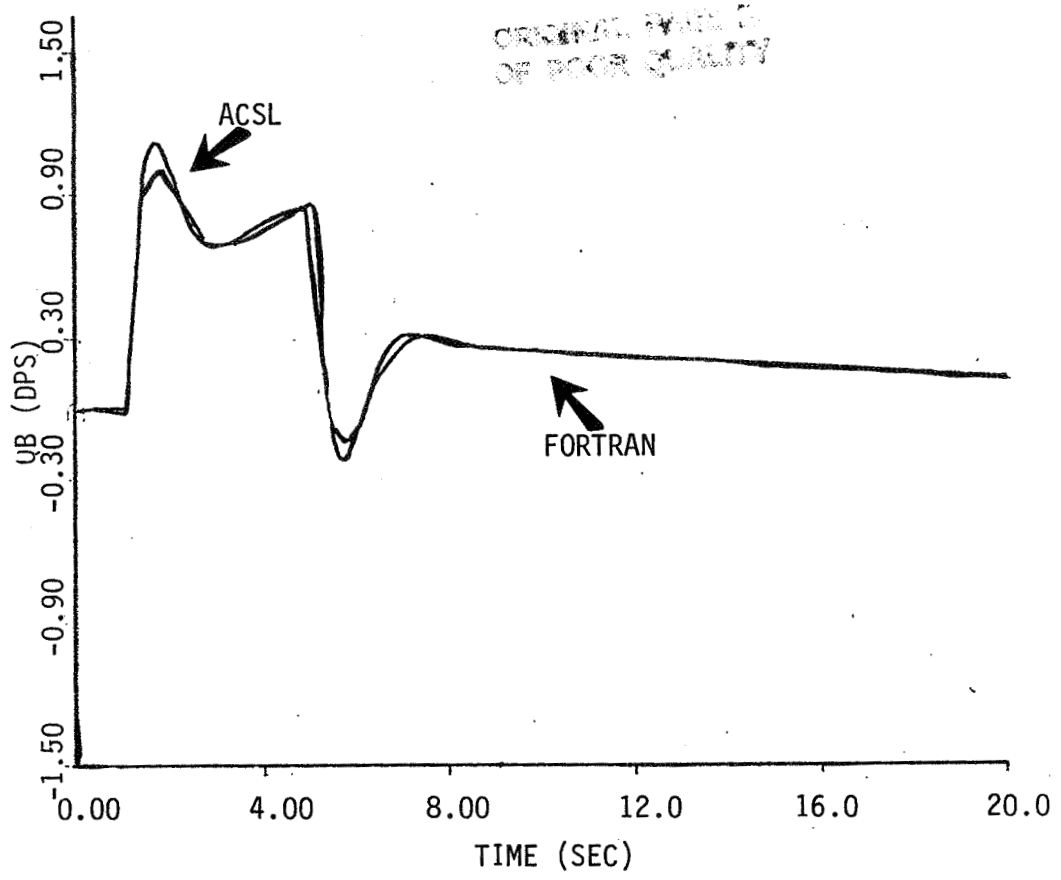

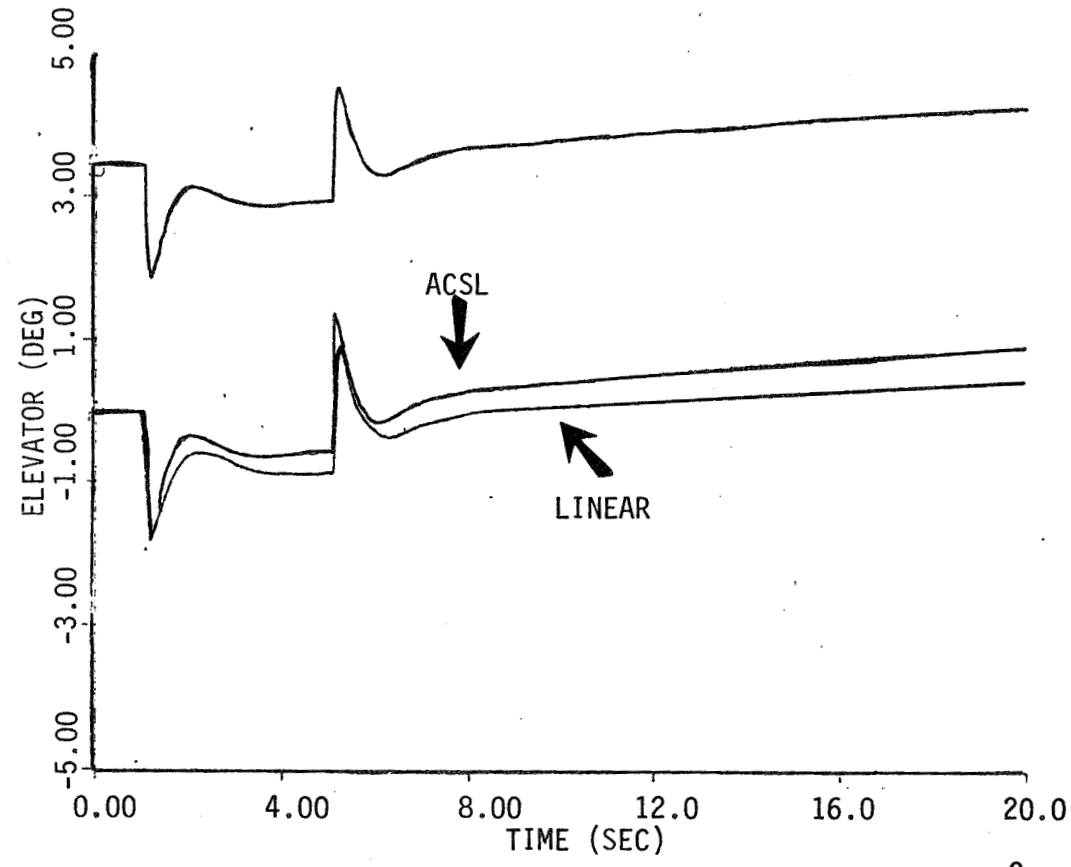

FIGURE 12 SIMULATION RESPONSE FOR A $\Delta\ddot{h}_c$ COMMAND OF 2.0 FPS^2.

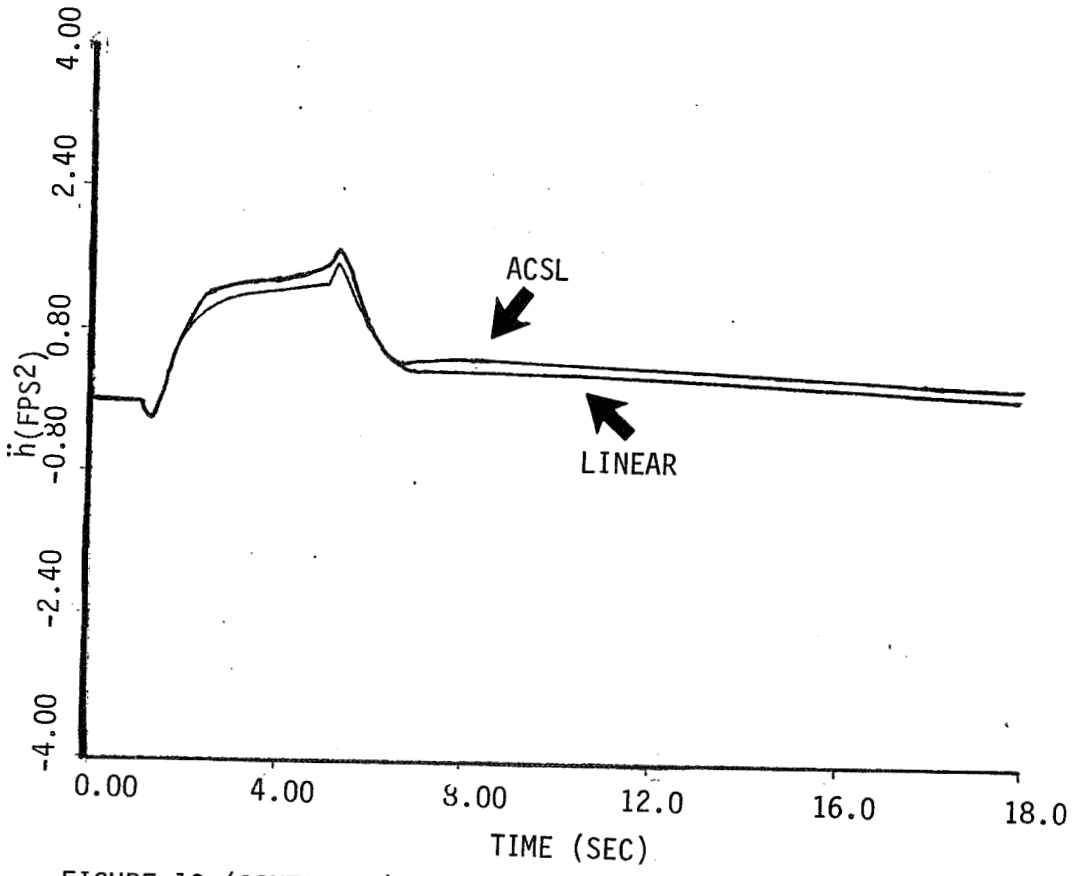

FIGURE 12 (CONTINUED) SIMULATION RESPONSE FOR A $\Delta\ddot{h}_c$ COMMAND OF 2.0 FPS^2.

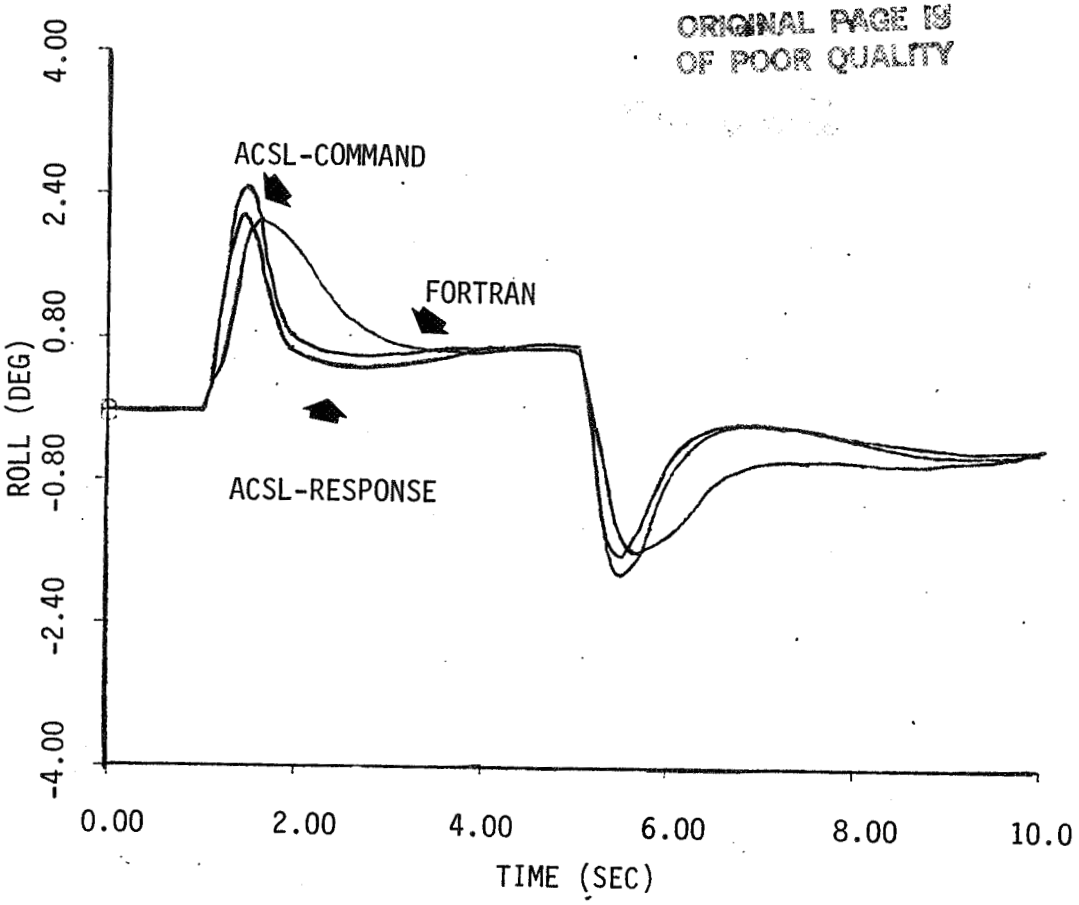

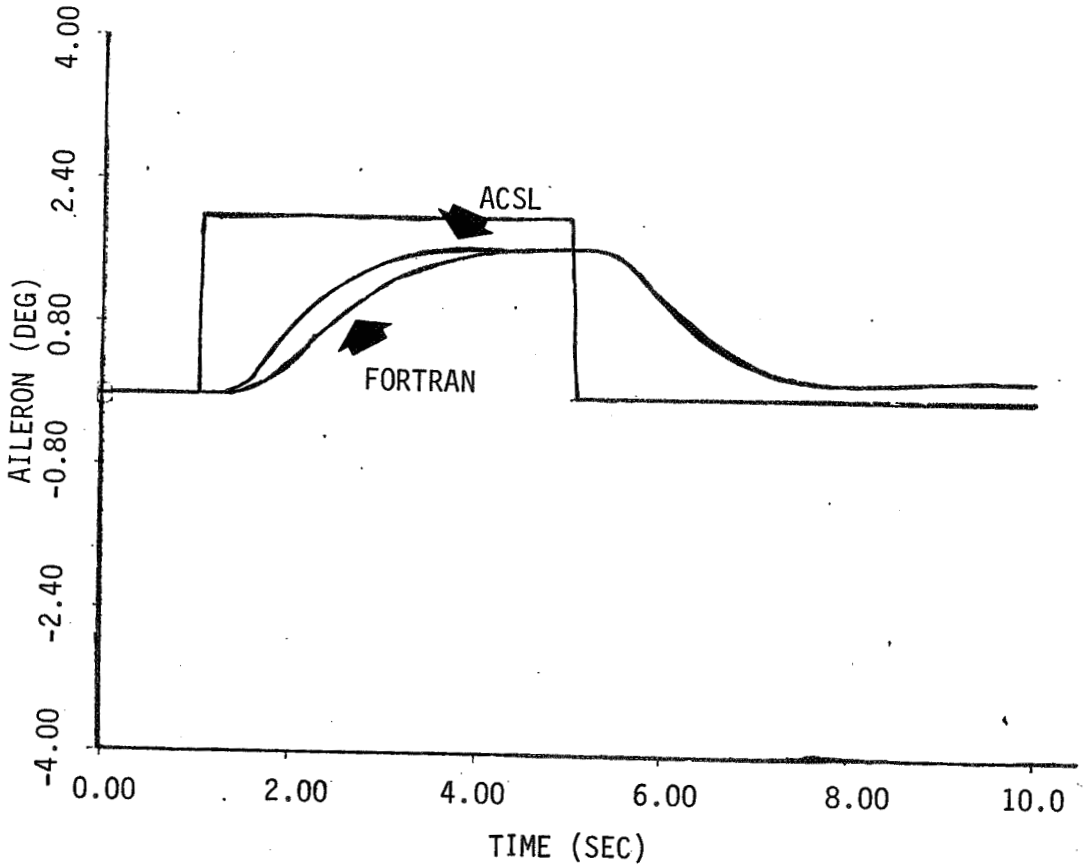

FIGURE 13 SIMULATION COMPARISON FOR A ϕ_C COMMAND OF 2.0 DEG.

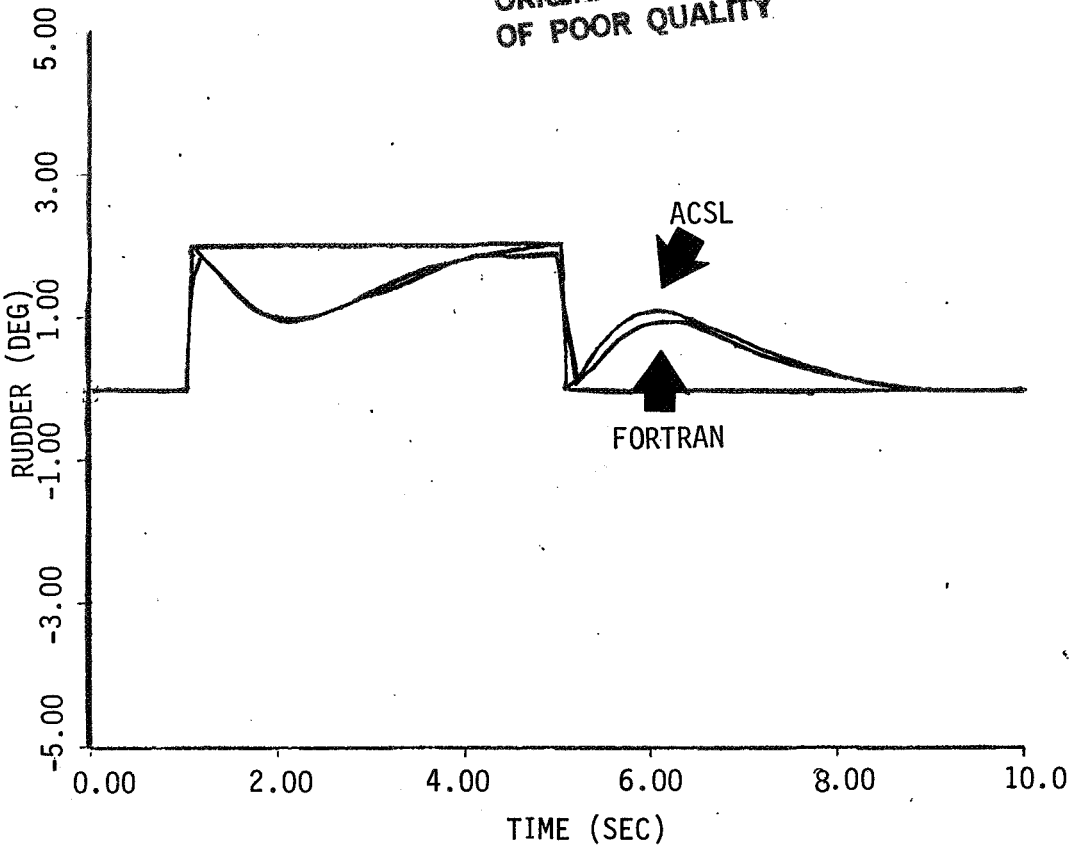

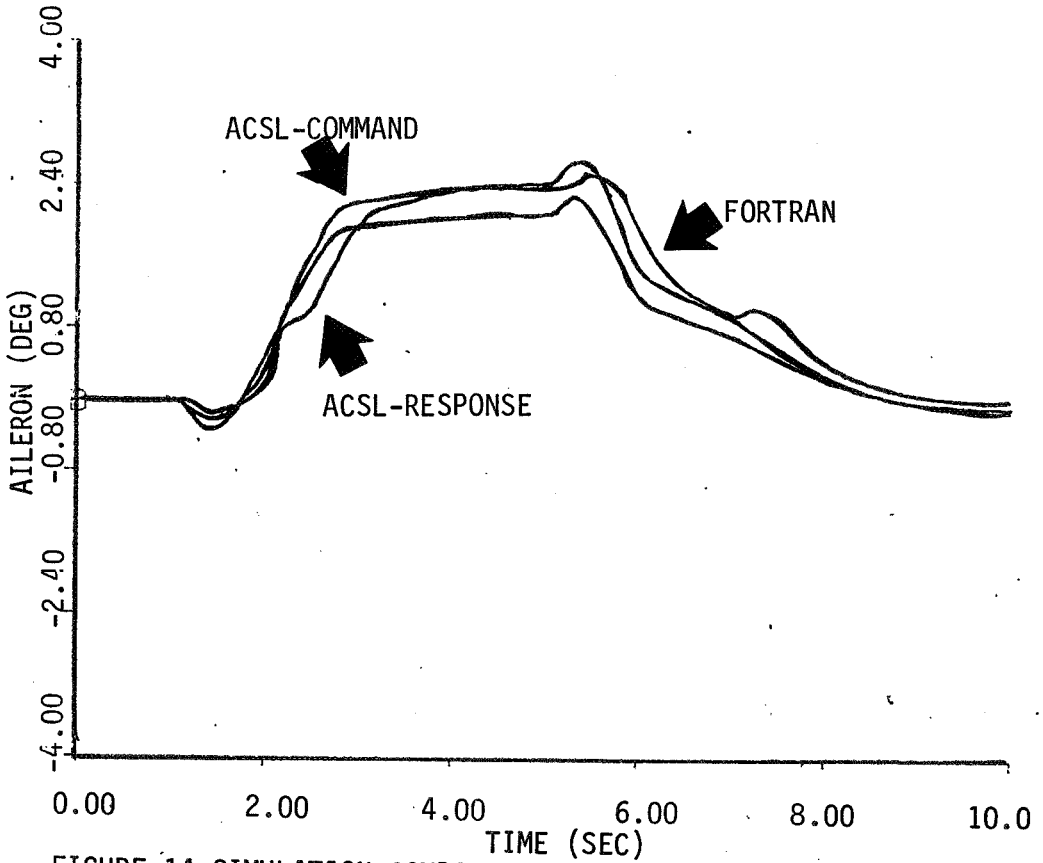

FIGURE 14 SIMULATION COMPARISON FOR A U_c COMMAND OF 2.0 DEG.

1. Report No.	2. Government Accession No.	3. Recipient's Catalog No.
NASA CR-166055		

4. Title and Subtitle	5. Report Date
ATOPS B-737 INNER-LOOP CONTROL SYSTEM LINEAR MODEL CONSTRUCTION AND VERIFICATION	FEBRUARY 1983
	6. Performing Organization Code
7. Author(s)	8. Performing Organization Report No.
JOHN R. BROUSSARD	TR 682101
	10. Work Unit No.
9. Performing Organization Name and Address	11. Contract or Grant No.
INFORMATION & CONTROL SYSTEMS, INC. 28 RESEARCH DRIVE HAMPTON, VA 23666	NAS1-15759
	13. Type of Report and Period Covered
12. Sponsoring Agency Name and Address	CONTRACTOR REPORT
NATIONAL AERONAUTICS & SPACE ADMINISTRATION WASHINGTON, DC 20546	14. Sponsoring Agency Code

15. Supplementary Notes

LANGLEY TECHNICAL MONITOR: RICHARD M. HUESCHEN
INTERIM REPORT

16. Abstract

Nonlinear models and block diagrams of an inner-loop control system for the ATOPS B-737 Research Aircraft are presented. Continuous-time linear model representations of the nonlinear inner-loop control systems are derived. Closed-loop aircraft simulations comparing nonlinear and linear dynamic responses to step inputs are used to verify the inner-loop control system models.

17. Key Words (Suggested by Author(s))	18. Distribution Statement
AIRCRAFT INNER-LOOP MODELING AIRCRAFT SIMULATION	UNCLASSIFIED - UNLIMITED SUBJECT CATEGORY 08

19. Security Classif. (of this report)	20. Security Classif. (of this page)	21. No. of Pages	22. Price
UNCLASSIFIED	UNCLASSIFIED	65	A04

For sale by the National Technical Information Service, Springfield, Virginia 22161